Protection Challenges and Solutions for AC Systems with Renewable Energy Sources: a Review

Zhe Yang, *Member*, *IEEE*, Hongyi Wang, *Student Member*, *IEEE*, Wenlong Liao, *Member*, *IEEE*, Claus Leth Bak, *Senior Member*, *IEEE*, and Zhe Chen, *Fellow*, *IEEE*

***Abstract*—Numerous renewable energy sources (RESs) are coupled with the power grid through power electronics to advance low-carbon objectives. These RESs predominantly connect to the AC collection network via inverters, with the electricity they produce either transmitted over long distances through high-voltage lines or utilized locally within the distribution system. The unique interfacing of RESs alters their fault response characteristics, typically resulting in limited fault currents, frequency deviations, and fluctuating sequence impedance angles. Therefore, existing protection principles based on fault signatures of synchronous generators will face significant challenges including distance relays, directional elements, differential relays, phase selectors, and overcurrent relays. To solve these issues, innovative protection technologies have been developed to bolster grid stability and security. Furthermore, the superior controllability of power converters presents an opportunity to devise effective control strategies that can adapt existing protection mechanisms to function correctly in this new energy landscape. Nevertheless, the complexity of fault behaviors exhibited by RESs necessitates further refinement of these schemes. Therefore, this paper aims to consolidate current research methodologies and explore prospective avenues for future investigation.**

***Index Terms*—Fault response characteristics, protection principles, renewable energy sources.**

I. Introduction

Driven by environmental protection imperatives and decreasing generation costs, renewable energy sources (RESs) have claimed an increasingly significant stake in the power system [1]–[3]. Notably, the Danish government has committed to transitioning to a fully renewable energy supply across all sectors by 2050, while China aims to achieve carbon neutrality by 2060 [4], [5]. This shift is steering the traditional electrical grid towards a power electronics-dominated system, precipitating a profound transformation in grid fault dynamics [6], [7]. Such transformations present a formidable challenge to the reliability of current protective relay operations [8].

Traditional protection methods are developed based on fault characteristics of synchronous generators (SGs) [9], [10]. These protection technologies developed for transmission networks primarily include differential protection, distance protection, directional elements, and phase selectors [11]. Differential protection serves as the principal protection for transmission lines, offering absolute selectivity and rapid response [12]. In a conventional network with power sources at both ends, the current phase angles are essentially identical for internal faults and the opposite for external faults. Consequently, the proportional restraint-based differential relay has operated with high reliability in the grid for many years [13]. Distance relays measure the fault distance from the fault point to the relay point and typically employ three zones with varying protection ranges and intentional time delays [14]. Among them, zone 3 functions as the backup protection for zone 1 and zone 2 [15]. Regarding directional elements, those used in the transmission grid are based on fault components [16]. Owing to the non-associated reference direction at the relay point, the sequence superimposed impedance angle calculated by these directional elements is close to −90° for forward directional faults and approximately 90° for reverse faults [17]. Moreover, the relative angle difference between sequence incremental currents varies across different regions depending on the fault type, forming the basis for the most commonly used phase selector [18]. Overcurrent relays are widely utilized in distribution networks due to their simplicity and effectiveness [19].

Initially, the impact of RESs on protection methods did not receive sufficient attention due to their low integration capacity [20]. As a result, RESs were required

Received: February 13, 2024
Accepted: August 1, 2024
Published Online: January 1, 2025
Zhe Yang is with the Department of Electrical and Electronic Engineering, Imperial College London, London SW7 2AZ, UK (e-mail: zhe.yang@imperial.ac.uk).
Hongyi Wang, Claus Leth Bak, and Zhe Chen are with AAU Energy, Aalborg University, Alborg 9220, Denmark (e-mail: howa@energy.aau.dk; clb@energy.aau.dk; zch@energy.aau.dk).
Wenlong Liao (corresponding author) is with the Wind Engineering and Renewable Energy Laboratory, École Polytechnique Fédérale de Lausanne, Lausanne 1015, Switzerland (e-mail: wenlong.liao@epfl.ch).
DOI: 10.23919/PCMP.2023.000279

to be disconnected from the service in the event of a fault. However, with the continuous increase in the share of RESs, such a practice now poses a serious challenge to the stability of the power system [21]. Modern grid codes mandate that RESs must ride through faults, leading to extensive discussions on the impact of fault ride-through (FRT) strategies on traditional protection methods [22]–[26]. RESs can be divided into full power converter interfaced sources (CIRESs) and partial power interfaced sources (PIRESs) [27], [28]. CIRESs primarily consist of permanent magnet synchronous generators (PMSGs)-based wind turbines and photovoltaic (PV) sources [25]. The power conversion section of PMSGs includes a source-side converter and a grid-side converter (GSC). The source-side converter regulates the active power harvested from the wind turbine and ensures a stable AC-side voltage. Meanwhile, the grid-side inverter is tasked with maintaining a constant DC voltage and managing reactive power injection [29]. The fault characteristics of CIRESs primarily rely on the grid-side inverter, so PV panels and wind turbines with the source-side converter are often equivalent to a controlled current source [7], [30]. Under this circumstance, the fault current of CIRESs is limited, and the sequence equivalent impedances are much larger than the line impedance and the equivalent grid's impedance. Additionally, the sequence impedance angles of CIRESs also vary with fault conditions [31], [23]. These phenomena significantly threaten the reliable operation of traditional protection relays.

Currently, the most widely used PIRESs are double-fed induction generators (DFIGs). To prevent serious overvoltage and overcurrent on the rotor side during bolted faults at the generator terminal, a crowbar device is often installed on the rotor side [32], [33]. When the crowbar device is activated, it short-circuits the rotor-side converter (RSC), causing the stator-side fault current to exhibit a rotor-speed-related frequency due to the loss of rotor-side excitation current [34], [35]. Additionally, the fault current displays a characteristic rapid decay [26]. As a result, all protection methods that rely on power frequency phasors will be adversely affected.

To address these issues, numerous protection schemes have been proposed, including the design of protection algorithms and control strategies. The first approach involves developing new protection algorithms based on the novel fault signatures of RESs, but implementing these methods requires updating all protection devices, which entails significant investment [23], [26], [36]–[38]. An alternative approach is to mimic the fault characteristics of SGs to make CIRESs compatible with conventional protective relays by designing new control strategies [39]–[44]. This method takes advantage of the excellent controllability of CIRESs and represents a promising direction for a future power grid dominated by RESs, although its practical application in engineering remains a considerable challenge.

This paper is a review of the fault characteristics and protection technologies of RESs. The structure of RESs is introduced in Section II, and the specific fault characteristics are analyzed in Section III. After that, the influence of RES integration on protection is studied in Section IV, and new protection technologies applicable to RESs are summarized in Section V. Moreover, the current challenges and future perspectives are given in Section VI, and a conclusion is drawn in Section VII.

II. The Structure of RESs

In this part, the basic structure and the related control system of CIRESs and DFIGs will be introduced.

A. The Structure of CIRESs

For CIRESs, the GSC utilizes a three-phase two-level inverter, with the commonly used controllers being decoupled current control (DCC) and decoupled sequence control (DSC) [45].

1) DCC

Figure 1 shows the control diagram of the DCC. During normal operation, the constant DC voltage control is utilized to generate the active current reference value, I_{1dref} [41]. Sometimes, the *d*-axis current reference can be directly set to 1 for simplicity. However, once a fault occurs, the outer voltage loop is deactivated, and the current reference values for the inner current loop are directly determined based on the specific FRT strategy [42]. To achieve decoupling of the *dq* axis, a coupling term is introduced into the inner current loop. Furthermore, the grid-side voltage (highlighted in red) undergoes feedforward compensation within the inner current loop to counteract any grid disturbances [46], [47]. Subsequently, a three-phase modulation wave is generated and compared with the carrier wave to produce the trigger signal for the inverter. In this controller configuration, the *q*-axis leads the *d*-axis by 90°, positioning the voltage vector on the *d*-axis.

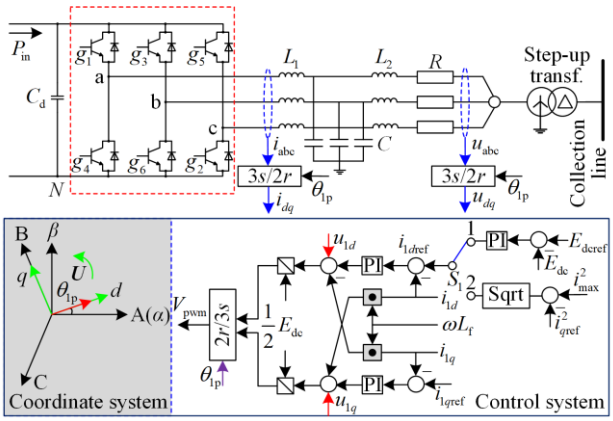

Fig. 1. The detailed topology of CIRESs based on DCC.

2) DSC

Various techniques are available for achieving separation of positive and negative sequences, including the

double second-order generalized integrator (DSOGI)-based method, the dual synchronous reference frame (DSRF)-based method, the one-quarter cycle ($T/4$) delay method, and the notch filter-based method [48], [49]. However, these methods introduce a delay in the controller's response, resulting in a slower reaction time compared to DCC. Specifically, for the $T/4$ delay method, the process of separation can be described as follows [50]:

$$\begin{pmatrix} i_{1d} \\ i_{1q} \end{pmatrix} = \boldsymbol{T}_{2\mathrm{s}-2\mathrm{r}} \frac{1}{2} \begin{pmatrix} i_\alpha - i_\beta \mathrm{e}^{-2\pi f_0 \frac{T_0}{4}\mathrm{j}} \\ i_\beta + i_\alpha \mathrm{e}^{-2\pi f_0 \frac{T_0}{4}\mathrm{j}} \end{pmatrix} \tag{1}$$

$$\begin{pmatrix} i_{2d} \\ i_{2q} \end{pmatrix} = \boldsymbol{T}_{2\mathrm{s}-2\mathrm{r}} \frac{1}{2} \begin{pmatrix} i_\alpha + i_\beta \mathrm{e}^{-2\pi f_0 \frac{T_0}{4}\mathrm{j}} \\ i_\beta - i_\alpha \mathrm{e}^{-2\pi f_0 \frac{T_0}{4}\mathrm{j}} \end{pmatrix} \tag{2}$$

where $\boldsymbol{T}_{2\mathrm{s}-2\mathrm{r}}$ is the transformation matrix from $\alpha\beta$ frame to the dq frame; T_0 is one cycle that is equal to 20 ms for the fundamental frequency f_0 of 50 Hz; i is the measured current; and its subscripts 1 and 2 represent positive- and negative-sequence components.

Figure 2 shows the control diagram when the $T/4$ delay method is employed, with the positive-sequence voltage aligned along the positive-sequence d-axis.

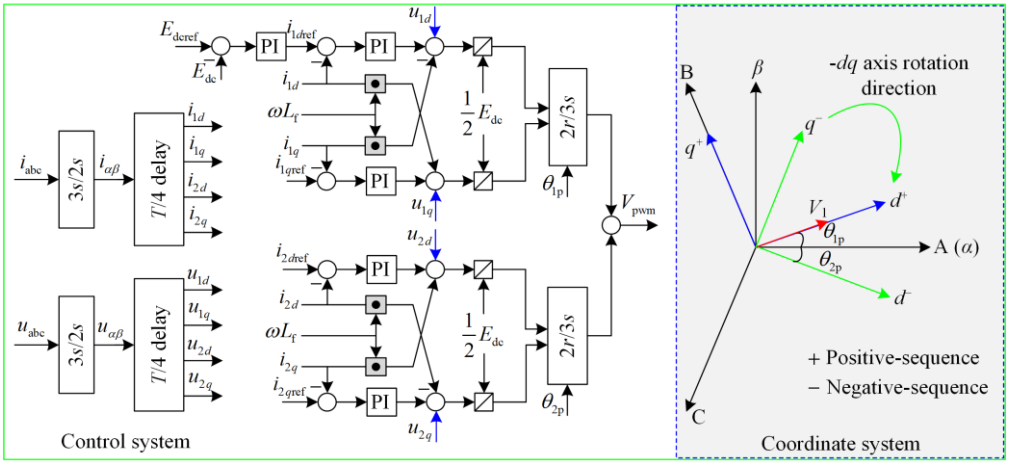

Fig. 2. The detailed diagram for DSC control.

Additionally, a negative-sequence control loop is incorporated as shown in Fig. 3, enabling the controller to achieve versatile fault control objectives. When direct power control is implemented, this controller can realize the following objectives: 1) suppressing the negative-sequence current; 2) suppressing active power oscillations; and 3) suppressing reactive power oscillations. Under this circumstance, the control equation can be expressed as [51]:

$$\begin{bmatrix} i_{1d\mathrm{ref}} \\ i_{1q\mathrm{ref}} \\ i_{2d\mathrm{ref}} \\ i_{2q\mathrm{ref}} \end{bmatrix} = \frac{2}{3} \begin{bmatrix} u_{1d} & u_{1q} \\ u_{1q} & -u_{1d} \\ -Ku_{2d} & Ku_{2q} \\ -Ku_{2q} & -Ku_{2d} \end{bmatrix} \begin{bmatrix} \frac{P_0}{M} \\ \frac{Q_0}{N} \end{bmatrix} \tag{3}$$

where K denotes the control factor which is chosen from 0, 1, and −1 corresponding to the above three control strategies; u and i are the measured voltage and current, and subscripts 1 and 2 represent positive- and negative-sequence components; P_0 and Q_0 are active and reactive power references; M and N are represented as follows:

$$\begin{cases} M = (u_{1d})^2 + (u_{1q})^2 - K\left[(u_{2d})^2 + (u_{2q})^2\right] \\ N = (u_{1d})^2 + (u_{1q})^2 + K\left[(u_{2d})^2 + (u_{2q})^2\right] \end{cases} \tag{4}$$

In addition, positive- and negative-sequence current references can also be settled directly using the specific FRT strategy such as the standard VDE-AR-N 4120 [52].

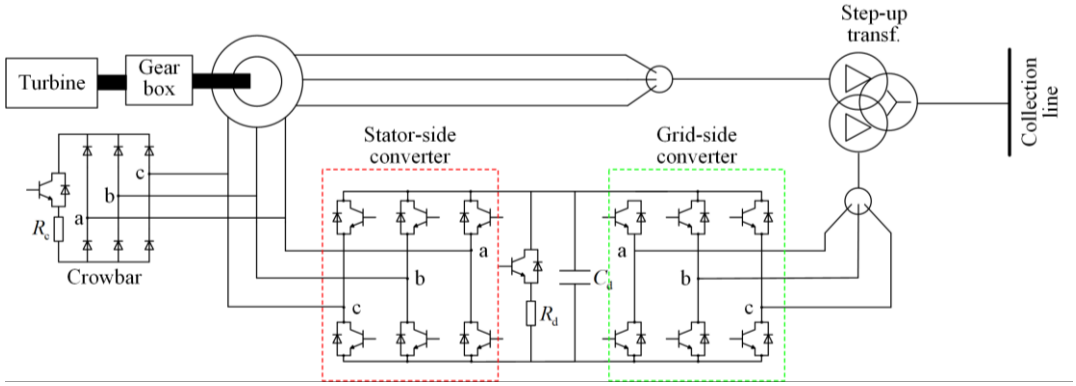

Fig. 3. The detailed topology for a DFIG.

B. The Structure of DFIGs

The basic structure of DFIGs is depicted in Fig. 3. The stator is directly connected to the grid, while the rotor is coupled to the grid through a back-to-back converter [53]. The controller for the GSC of DFIGs is the same as that used for CIRESs. The RSC primarily functions to generate the excitation current at slip frequency, enabling the DFIGs to maintain power frequency current on the stator side under both super-synchronous and sub-synchronous conditions. Typically, the slip, s ranges from −30% to 30% [54]. To prevent serious overvoltage and overcurrent on the rotor side, a crowbar device is installed on the rotor side. Additionally, a chopper circuit is implemented to protect the DC capacitor from damage due to overvoltage [55].

Figure 4 illustrates the controller of the RSC, where the *d*-axis is aligned with the stator voltage vector. In the figure, ω_2 is the slip angular velocity, L_m denotes the magnetizing inductance, U_s is the stator voltage, the subscripts 's' and 'r' denote the stator- and rotor-side quantities, and $\sigma = 1 - L_m^2/(L_s L_r)$.

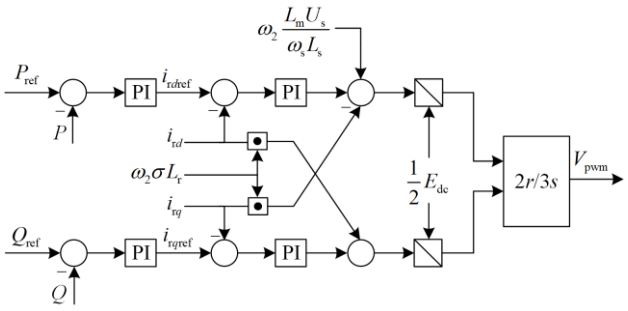

Fig. 4. The detailed controller of the RSC for a DFIG.

When the terminal voltage falls below 0.9 p.u., DFIGs will enter the FRT state [56]. In this situation, the power outer loop is disconnected, and only the inner rotor current control loop needs to be considered. It is important to note that the short-circuit process under study is so brief that the rotor's rotational speed is generally assumed to be constant for the analysis [57]. Once the crowbar device is activated, the RSC will be bypassed. Similarly, the RSC can also employ a DSC-based controller, allowing for flexible control objectives, such as eliminating electromagnetic torque oscillations and complying with IEEE Std 2800-2022 [58], [59].

III. Fault Characteristic Analysis

In this part, the fault behaviors of RESs will be studied, and they are significantly different from those of SGs due to the unique structure and control system.

A. CIRESs

1) DCC Control

In compliance with most grid codes, CIRESs are mandated to inject reactive current into the grid during a fault, although the specific regulations may vary slightly [25], [60]. The Danish FRT strategy in Fig. 5 serves as an example. The reactive current (i_{1qref}) is determined based on voltage sags in Fig. 5(a), and the remaining capacity is used to generate the active current (i_{1dref}). When the positive-sequence voltage falls within area A in Fig. 5(b), CIRESs can continue normal operation. If CIRESs are operating at area B, they are required to maintain a grid-connected state for a specified duration. In the case of area C, they are permitted to disconnect from the grid [60].

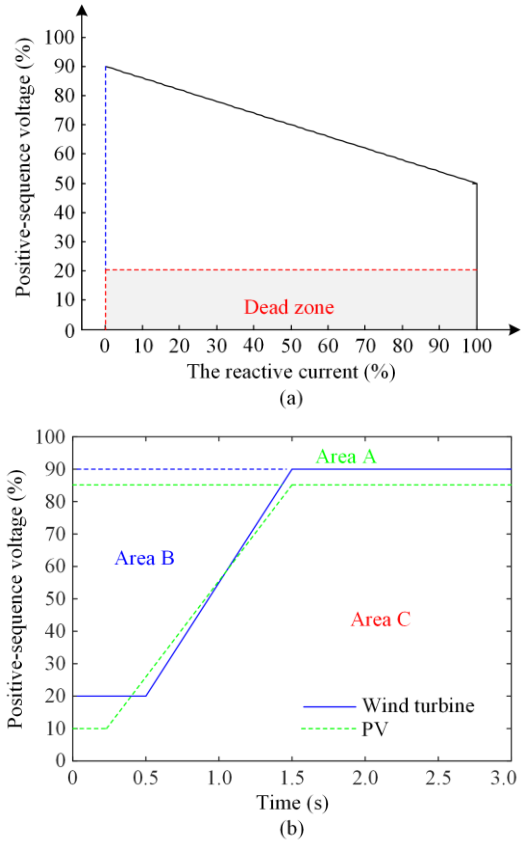

Fig. 5. FRT requirement in Denmark. (a) Reactive current. (b) The time-voltage profile.

The maximum fault current from CIRESs is typically 1.2 to 1.5 times the rated current to protect the full-power inverter. When a line-B-to-line-C (BC) fault occurs at the middle point of L_{12} (see Fig. 10), the fault voltage, current references, and fault currents are displayed in Fig. 6.

It can be seen from Fig. 6(b) that i_{1qref} is set based on the voltage sags depicted in Fig. 6(a), and the active current is calculated using the remaining capacity. Under this circumstance, the three-phase fault currents in Fig. 6(c) will be equal to 1.2 times the rated current during the steady state. In addition, there is a short transient period of about 20 to 30 ms, which is an uncontrollable process. Since there is no negative-sequence current injection, three-phase fault currents remain balanced during this asymmetrical fault.

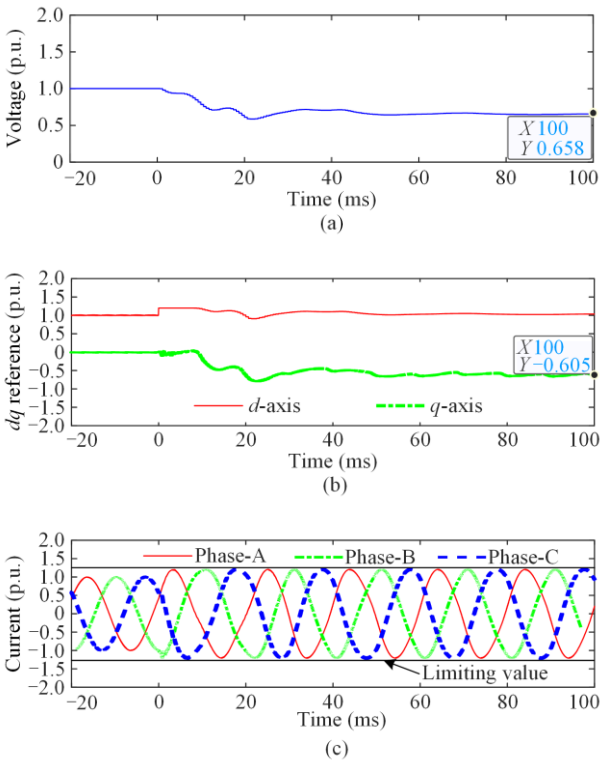

Fig. 6. The related measurements for a BC fault. (a) Positive-sequence voltage. (b) Current references. (c) Three-phase current.

For the fault steady state, the fault current is regulated by current command values, so the phase-A current can be expressed as [61]:

$$i_{\mathrm{a1}}=\sqrt{i_{1d\mathrm{ref}}^2+i_{1q\mathrm{ref}}^2}\cos\left(\omega t+\theta_{\mathrm{1p}}+\arctan\left(\frac{i_{1q\mathrm{ref}}}{i_{1d\mathrm{ref}}}\right)\right) \quad (5)$$

where ω is the synchronized angular velocity; and θ_{1p} is the phase angle detected by the phase-locked loop (PLL).

For the transient process, the current expression depends on the controller parameters. When the proportional and the integral coefficients are tuned according to (6), the system can be reduced to a first-order model, so the *dq*-axis fault currents can be expressed as (7) [62].

$$\begin{cases} k_{\mathrm{ip}}=\omega_{\mathrm{c}}L_{\mathrm{f}} \\ k_{\mathrm{ii}}=\omega_{\mathrm{c}}R \end{cases} \quad (6)$$

where k_{ip} and k_{ii} are respectively the proportional and integral constants; L_{f} and R are the filter total inductor and resistance of the inverter; and ω_{c} is the open loop crossover frequency of the first-order system.

$$\begin{cases} i_d(t)=i_{d\mathrm{ref}}-(i_{d\mathrm{ref}}-i_{d(0)})\mathrm{e}^{-\omega_{\mathrm{c}}t} \\ i_q(t)=i_{q\mathrm{ref}}-(i_{q\mathrm{ref}}-i_{q(0)})\mathrm{e}^{-\omega_{\mathrm{c}}t} \end{cases} \quad (7)$$

where $i_{d(0)}$ and $i_{q(0)}$ are the initial value of *dq-axis* currents.

If the saturation element is placed after the PI loop, it will prolong the current transient process. In such cases, the fault current will exhibit a peak value, and the specific expression for the transient current is calculated in [62]–[64]. In addition, the dynamic feature of the PLL will also influence the transient current from CIRESs, but the impact is limited for the DCC control due to the fast-tracking speed of the traditional PLL [35].

2) DSC Control

In the standard VDE-AR-N 4120 [52] in Fig. 7, the negative-sequence reactive current is also required to be injected into the grid [52]. Consequently, it is necessary to add a negative-sequence control loop. For this FRT strategy, the positive-sequence reactive current reference is still determined based on the positive-sequence voltage variation during and before a fault. Additionally, $i_{2d\mathrm{ref}}$ and $i_{2q\mathrm{ref}}$ are set according to the corresponding negative-sequence *q*-axis and *d*-axis voltage components during a fault. In this situation, the negative-sequence impedance angle will be equal to 90°, similar to that of SGs [65]. The remaining capacity will be used to generate $i_{1d\mathrm{ref}}$.

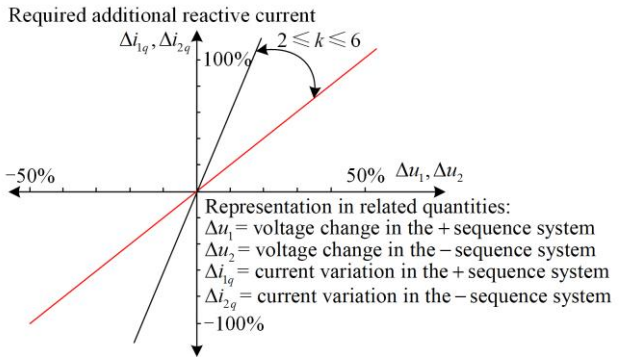

Fig. 7. The standard VDE-AR-N 4120.

In some cases, the calculated current references will make three-phase fault currents exceed the current limit value. Under this circumstance, they need to be scaled down in proportion [39]. In addition, it is generally believed that there is no room to generate $i_{1d\mathrm{ref}}$ [66], [67]. However, reference [68] points out the suitable $i_{1d\mathrm{ref}}$ can even reduce the fault current amplitude, and proposes a new algorithm to generate the maximum $i_{1d\mathrm{ref}}$ when reactive power priority and the current limiting are satisfied.

The negative-sequence current expression during the steady state can be expressed as:

$$i_{\mathrm{a2}}=\sqrt{i_{2d\mathrm{ref}}^2+i_{2q\mathrm{ref}}^2}\sin\left(\omega t-\theta_{\mathrm{2p}}-\arctan\left(\frac{i_{2q\mathrm{ref}}}{i_{2d\mathrm{ref}}}\right)+90°\right) \quad (8)$$

where θ_{2p} is equal to the opposite number of θ_{1p}.

Under this circumstance, the phase fault currents during the steady state [40] are:

$$\begin{cases} |I_{\mathrm{WA}}| = \sqrt{|I_1|^2 + |I_2|^2 + 2|I_1||I_2|\cos\Delta\beta} \\ |I_{\mathrm{WB}}| = \sqrt{|I_1|^2 + |I_2|^2 - 2|I_1||I_2|\cos(\Delta\beta - 60°)} \\ |I_{\mathrm{WC}}| = \sqrt{|I_1|^2 + |I_2|^2 - 2|I_1||I_2|\cos(\Delta\beta + 60°)} \end{cases} \quad (9)$$

where I_1 and I_2 are positive- and negative-sequence fault currents; subscript 'WA', 'WB' and 'WC' denote the quantities of phase A, B, and C on the RES side; and $\Delta\beta$ is the angle disparity between positive- and negative-sequence currents.

During the transient process, the fault current is affected by the positive- and negative-sequence separation mode (PNSM). The DSOGI-based method is a commonly used approach for achieving this, with its basic structure depicted in Fig. 8.

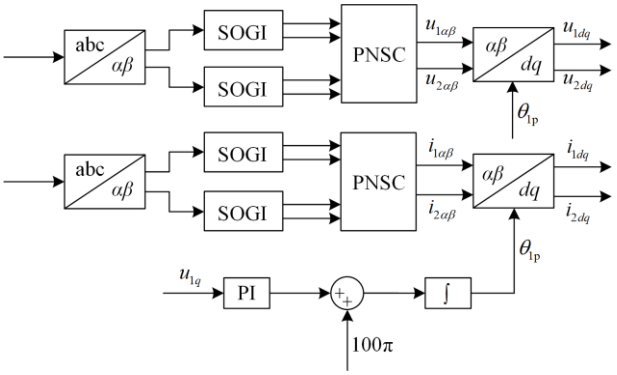

Fig. 8. The diagram of the DSOGI-PLL [45].

At this time, when the DSOGI-based method is used [45], the system model can be expressed as:

$$\frac{1}{P(s)}\boldsymbol{E}I_{dq}(s) = (i_{dq\mathrm{ref}}(s) - \boldsymbol{H}I_{dq}(s))PI(s) + (\boldsymbol{H} - \boldsymbol{E})I_{dq}(s) \quad (10)$$

where $\boldsymbol{E}$ is the identity matrix; $\boldsymbol{H}$ is the transfer function of the DSOGI-PLL; $I_{\mathrm{dq}}(s)$ is the output from the current controller; $PI(s)$ is the transfer function of the PI loop; and $P(s)$ can be expressed as:

$$P(s) = \frac{1}{R} \times \frac{1}{\tau s + 1} \quad (11)$$

where τ is equal to L/R; and R and L are the resistance and inductance between PCC and the inverter terminal.

After that, the balancing-free square-root algorithm in [69] is used to simplify the transfer function of $H(s)$, followed by the use of the inverse Laplace transform to derive the time-domain expression for the fault current. Similarly, the mathematical model of the system is established in [49] for other PNSMs such as the $T/4$ delay method, the DSRF-based method, and the notch filter-based method. The fault current calculation process is similar to [45].

In conclusion, CIRESs are a controlled current source and the fault behaviors are summarized in Table I for the fault occurring on the high-voltage (HV) transmission line. In this table, A, B, and C denote the faulty phase, and G means line to ground. In addition, Δf denotes the frequency offset.

TABLE I
FAULT BEHAVIORS OF CIRESS

Control	Fault type	I_1	I_2	I_0 at HV	Δf
DCC	AG and BCG	Yes	No	Yes	Small
	BC and ABCG	Yes	No	No	Small
DSC	AG and BCG	Yes	Can	Yes	Small
	BC	Yes	Can	No	Small
	ABCG	Yes	No	No	Small

B. DFIGs

The fault current of DFIGs can be discussed according to the crowbar operating status.

1) The Crowbar Device Is Activated

At this point, the rotor side is short-circuited, and the back-to-back converter is blocked. In this case, the fault current of DFIGs is the same as that of the squirrel cage induction generators (SCIGs) when a severe three-phase fault occurs [70]:

$$i_{\mathrm{f\_DF}}(t) = \frac{V_{\mathrm{p}}}{1-s}\left(\frac{1}{X_{\mathrm{t}}} - \frac{1}{X_{\mathrm{LS}} + 1.5X_{\mathrm{MS}}}\right)\mathrm{e}^{-t/T_{\mathrm{r}}} \times \cos((1-s)\omega t + \theta_0) + \frac{V_{\mathrm{p}}}{1-s}\left[\frac{1}{X_{\mathrm{t}}}\mathrm{e}^{-t/T_{\mathrm{a}}}\cos(\theta_0)\right] \quad (12)$$

where V_{p} represents the induced voltage amplitude; X_{t} is the transient reactance of SCIGs; X_{LS} and X_{MS} are the leakage reactance and the magnetizing reactance; s represents the slip of the SCIG with a range from –30% to 30%; T_{a} and T_{r} are the stator time constant and the short-circuit transient time constant; and θ_0 denotes the fault inception angle.

It can be seen from (12) that the rotor-speed-frequency component will dominate the DFIG fault current. Meanwhile, the small T_{r} also leads to the fast decay of this sine wave.

When an unbalanced fault arises and the crowbar resistance is considered, the positive- and negative-sequence fault circuits of DFIGs can be equivalent to an impedance model, and they are [58]:

$$Z_{\mathrm{DFIG1}} = R_{\mathrm{s}} + \mathrm{j}\omega L_{\mathrm{s}}\frac{\mathrm{j}s\omega\sigma L_{\mathrm{r}} + R_{\mathrm{ra}}}{\mathrm{j}s\omega L_{\mathrm{r}} + R_{\mathrm{ra}}} \quad (13)$$

$$Z_{\mathrm{DFIG2}} = R_{\mathrm{s}} + \mathrm{j}\omega L_{\mathrm{s}}\frac{\mathrm{j}(2-s)\omega\sigma L_{\mathrm{r}} + R_{\mathrm{ra}}}{\mathrm{j}(2-s)\omega L_{\mathrm{r}} + R_{\mathrm{ra}}} \quad (14)$$

where R_{ra} is equal to $(R_{\mathrm{r}} + R_{\mathrm{c}})$; and R_{c} is the crowbar resistance.

2) The Crowbar Device Is Not Activated

The excitation current produced by the rotor-side converter (RSC) still helps the stator-side current

maintain the power frequency. In this situation, the fault current should include two parts: the stator-side current and the fault current from the GSC. The stator-side current is expressed (15) for a minor three-phase fault if the inner rotor current controller is designed to a first-order system for three-phase faults [57]:

$$i_{sa}(t) = D\sin(\varphi - \theta_0)e^{-R_s t/L_s} + I\cos(\omega t + \theta_0 + \gamma) \quad (15)$$

where D and I are the magnitudes of DC and AC components respectively; φ and γ are two phase angles related to controller parameters and the parameters of SCIGs; R_s and L_s are the resistance and the inductance of the stator winding.

As found in (15), the stator-side current contains only a damped DC component and a stable fundamental frequency AC component. If the inner rotor control loop is equivalent to a typical second-order system, the stator current expression is similar to (15). Only the amplitude of the DC component is different [57].

The fault current expression of the GSC is like that of the CIRES due to the same structure and controller. However, the maximum capacity of the GSC only accounts for 30% of the total capacity of DFIGs, so the DFIG fault current is dominated by the stator-side current [54]. When the fault current from the GSC is also considered, the detailed fault model of DFIGs is drawn in Fig. 9. In the figure, Z_f is the filter impedance, $\dot{I}_g$ is the GSC current, and $L_{1s} = L_s - L_m$, $L_{1r} = L_r - L_m$ [58].

Different control objectives can be achieved by designing different current references of the RSC and GSC, so the fault behavior will depend on the specific control strategy. Compared with CIRESs, the unique fault behavior is the frequency offset phenomenon when the crowbar device is triggered.

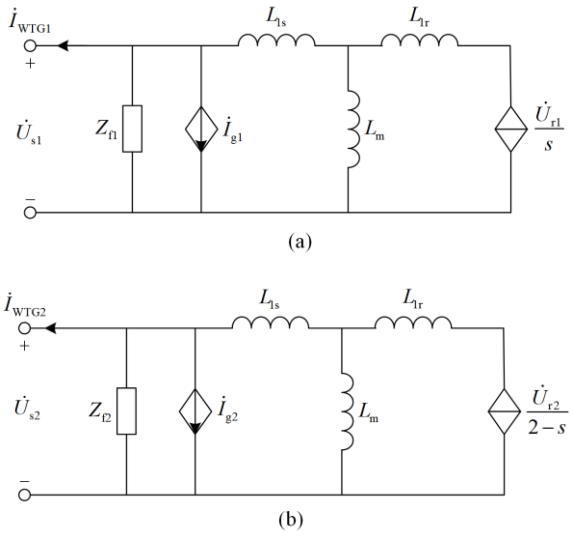

Fig. 9. The sequence fault circuit of the DFIG. (a) Positive-sequence. (b) Negative-sequence.

IV. Protection Challenges

After summarizing these new fault characteristics, this section analyses their impact on traditional protective relays including differential relays, directional elements, phase selectors, distance relays, and overcurrent relays.

A. Differential Protection

RESs are connected to the collection line through a step-up transformer. Once the power energy is generated, it is conveyed to the remote grid via the transmission line, as illustrated in Fig. 10.

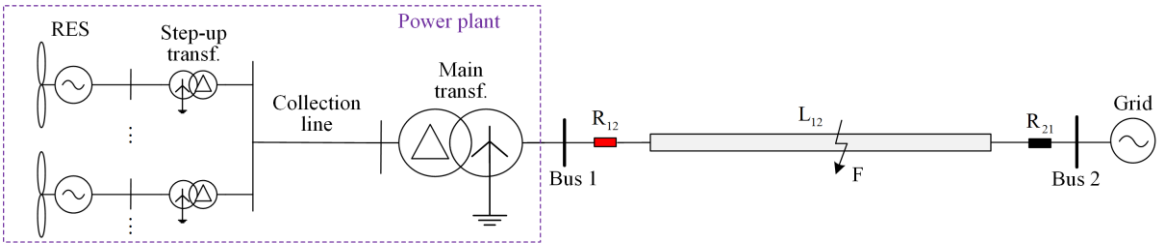

Fig. 10. The transmission line with a RES power plant.

In traditional transmission networks, the fault currents on both sides have a similar phase angle for internal faults, thus the basic criterion for proportional restraint differential protection is as follows [71]:

$$\begin{cases} I_D \geqslant I_{D0} \ \& \ I_D \geqslant k_u I_R \\ I_D = \left|\dot{I}_S + \dot{I}_W\right| \\ I_R = \left|\dot{I}_S - \dot{I}_W\right| \end{cases} \quad (16)$$

where I_D and I_R are respectively the operating current and the restraint current; I_{D0} denotes the starting current; $\dot{I}_S$ and $\dot{I}_W$ are the grid-side and the RES-side current phasors; and k_u is the restraint coefficient which ranges from 0.1 to 0.8.

When CIRESs with DCC are integrated, the fault current from CIRESs will remain balanced for all types of faults [25]. At this point, the fault current angle difference on both sides can be greater than 90° such that the sensitivity of differential protection will be reduced for BC faults [47]. When a BC fault arises at the midpoint of L_{12}, the current angle and the performance of differential protection are shown in Fig.11.

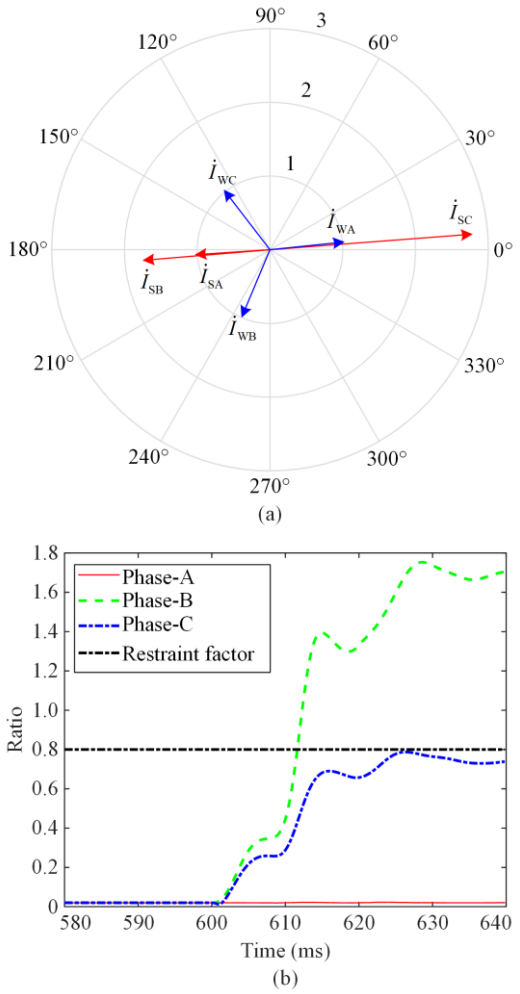

Fig. 11. The related measurements of differential protection. (a) The phasor diagram. (b) The ratio of the operating current to restraint current.

As shown in Fig. 11(a), the current angle difference for phase-C is close to 120°, so the ratio of the operating current to the restraint current will be lower than the restraint factor in Fig. 11(b) such that differential protection has a low sensitivity level and even fails to operate.

For DFIGs, when the crowbar device is triggered, the DFIG current angle extracted by fast Fourier transform (FFT) will change periodically due to the spectrum leakage caused by the non-fundamental frequency fault current [26]. At this time, the ratio of the operating current to the restraint current will also change periodically, so it can sometimes be lower than the restraint coefficient such that differential protection will not be activated [30]. In addition to using the phase current, the negative-sequence current can also be used to construct differential protection. Currently, the performance of this differential protection depends on the negative-sequence equivalent impedance. When the control strategy of eliminating the double grid frequency oscillations in electromagnetic torque is adopted, the negative-sequence equivalent impedance represents a capacitive feature, so the negative-sequence component-based differential protection may fail to be triggered [72]. In addition, the zero-sequence current can also be utilized to form a differential protection method, but it is only applicable to unbalanced earth faults.

B. Directional Elements

Fault component-based directional elements are frequently employed in transmission networks including positive-sequence fault component-based directional elements, negative-sequence directional elements, and zero-sequence directional elements [23]. They are designed according to the sequence superimposed impedance angle of the backside system:

$$Z_\phi = \frac{\Delta \dot{U}_\phi}{\Delta \dot{I}_\phi} \tag{17}$$

where the subscript ϕ denotes the sequence components; and Δ is the fault incremental component.

Due to the function of the magnetic loop for SGs, the sequence-superimposed impedance of SGs is always dominated by the inductive reactance, so the sequence-superimposed impedance angle of SGs is close to 90°. Since the non-associated reference direction is used at the relay point, the protection criterion for forward faults [17] is given as:

$$-180° < \arg Z_\phi < 0° \tag{18}$$

For a fault on the transmission line in Fig. 10, the zero-sequence fault loop only includes the part of the transmission line and the main transformer and is not related to the source impedance so that zero-sequence directional elements can work properly for asymmetrical ground faults. However, positive-sequence fault component-based directional elements and negative-sequence directional elements are affected since the positive- and negative-sequence fault loops will include the CIRES equivalent superimposed impedance whose angle is determined by the FRT strategy. References [16] and [23] have studied the impedance behavior when the direct power control in (3) is used, which shows that the superimposed impedance angles will change from −180° to 180° under different fault conditions. In addition, the current references can also be given directly according to grid codes. Reference [73] points out that directional elements may not be triggered for forward faults when the grid code in Denmark is used. In addition, negative-sequence directional elements may report a positive directional fault for reverse faults, resulting in false tripping [74].

For DFIGs, the superimposed impedance angle will also deviate from 90° if the crowbar circuit is not activated since the current reference change of the RSC will lead to a variable internal potential [57]. When the crowbar circuit is activated, the terminal voltage is at the fundamental frequency, but the fault current from DFIGs is at the non-fundamental frequency [75], [76].

In this situation, the impedance angle (the ratio of voltage to current) will be variable from −180° to 180°, causing directional elements not to work properly [77].

C. Phase Selectors

The phase selector can be divided into the current amplitude-based method [78], and the current angle difference-based method [79]. For the current amplitude-based method, the phase with the maximum fault current is identified as the faulty phase. However, three-phase fault currents from CIRESs with DCC are symmetrical. In addition, the phase current amplitude for CIRESs with DSC depends on positive- and negative-sequence current references instead of fault types, so this kind of method is invalid for CIRESs.

The DFIG fault current amplitude is related to the fault types since there is an induced voltage source when the crowbar circuit is not triggered. However, the current amplitude-based method has a limited capacity to resist fault resistance [24]. Once the crowbar circuit is activated, the fast decay and frequency offset will influence the accuracy of the amplitude extraction and further affect the performance of the current amplitude-based phase selector.

In addition, the current angle-based phase selector is designed according to the relative angle between sequence incremental currents including the angle difference between negative- and positive-sequence incremental currents (δ_1) and the angle difference between negative- and zero-sequence incremental currents (δ_0), and the specific logic is shown in Fig. 12.

When CIRESs with DCC are integrated, there is no negative-sequence current inject ion from CIRESs, thus the extracted negative-sequence current angle is unstable such that this phase selector cannot work well. In some commercial relays, the negative-sequence current should be higher than 10% of the rated current to trigger the protection function, so the phase selector will not be activated in this case [74]. Moreover, positive- and negative-sequence currents are controlled by corresponding current command values if the DSC control is used, so δ_1 and δ_0 are no longer determined by fault types [40]. Under this circumstance, the phase selector may misjudge the fault type.

For DFIGs, the excitation current from RSC can be settled with different FRT strategies when the crowbar device is not activated, so incremental sequence currents may not follow the rule in Fig. 12. If the crowbar device is activated, the impedance model of DFIGs is related to the crowbar resistance [80]. The high crowbar resistance easily leads to misoperation of phase selectors. In addition, the non-fundamental frequency component will also affect its performance.

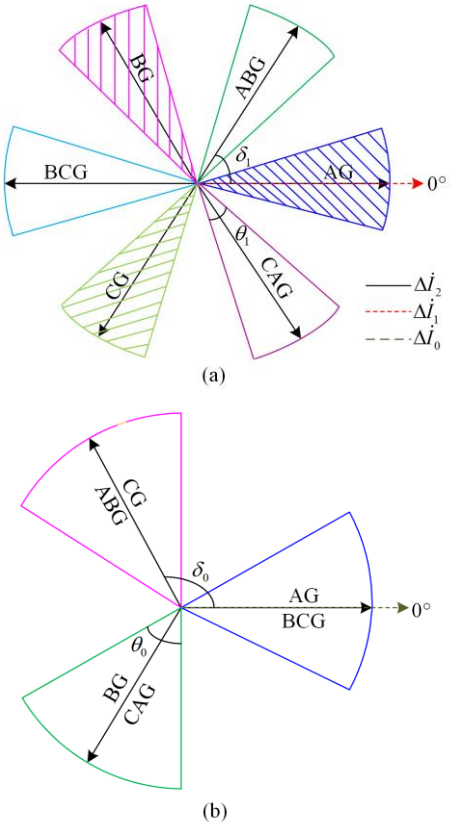

Fig. 12. The logic of the current angle-based phase selector. (a) δ_1. (b) δ_0.

D. Distance Relays

Distance relays are often used on the transmission line, and they can detect internal faults by calculating the apparent impedance [81]. To compute the fault impedance from the fault point to the relay point, there are two fault loops for different fault types: line-to-earth loop and line-to-line loop [22]. The line-to-earth loop is present for ground faults, and the measurements are $\dot{U}_\varphi$ and $\dot{I}_\varphi + k_0 3\dot{I}_0$ (k_0 denotes the zero-sequence compensation coefficient, and φ denotes the faulty phase). The line-to-line fault loop is present for line-to-line faults, line-to-line ground faults, and three-line ground faults, and the measurements are $(\dot{U}_\mathrm{B} - \dot{U}_\mathrm{C})$ and $(\dot{I}_\mathrm{B} - \dot{I}_\mathrm{C})$ for BC faults.

When CIRESs are connected, the apparent impedance of distance relays on the CIRES side is (17) for three-phase ground faults [8]:

$$Z_\mathrm{m} = \frac{\dot{U}_\mathrm{m}}{\dot{I}_\mathrm{m}} = Z_{k1} + \underbrace{\frac{\dot{I}_\mathrm{W} + \dot{I}_\mathrm{S}}{\dot{I}_\mathrm{W}}}_{M_\mathrm{T}} R_\mathrm{g} \tag{19}$$

where $\dot{U}_\mathrm{m}$ and $\dot{I}_\mathrm{m}$ respectively denote the measured voltage and the measured current of distance relays; Z_{k1} denotes the line fault impedance; and R_g denotes the fault resistance.

Since CIRESs are weak sources with a limited fault current, the grid-side fault current is far higher than the RES-side current such that the amplitude of M_T is much larger than 1. In this way, the influence of the fault resistance is amplified. In addition, the phase angle of $\dot{I}_W$ can lead or lag that of $\dot{I}_S$, so the additional impedance is a capacitive or inductive component. These factors will cause the misoperation of distance relays [22], [41]. Conversely, the distance relay on the grid side is less affected by the CIRES integration since M_T for the grid-side distance relay should be close to 1 such that the impact of R_g is not magnified [22]. Besides the apparent impedance-based implementation scheme, the distance relay can be implemented by the phase comparator and reactance method. For the phase comparator-based method, the distance relay can underreach for internal faults when the negative-sequence current is used for polarization, and it is prone to overreach for external faults if the zero-sequence current is adopted for polarization [82]. The performance of the reactance method depends on the correct evaluation of the current angle at the fault point. The reactance method can indicate the fault distance if the fault point current is approximated with the zero-sequence current, but it will not work properly if the negative-sequence current is used to evaluate the fault point current angle [83].

When DFIGs are integrated and the crowbar device is not activated, the fault current of DFIGs is still lower than that of the grid, so the weak infeed of DFIGs still influences the correct operation of distance relays. In addition, if the crowbar circuit is triggered, the apparent impedance will be rotated in a large scope so that the impedance trace may come into zone-1 of the local distance relay for the fault on the downstream line, leading to the wrong tripping and enlarging the outrage scope [54].

E. Overcurrent Relays

Overcurrent relays act as the main protection of distribution networks, and they include definite time overcurrent relays, instantaneous overcurrent relays, inverse time overcurrent relays, inverse definite minimum time (IDMT) overcurrent relays, very inverse time overcurrent relays, and extremely inverse time overcurrent relays [84].

The time-current characteristics for various inverse overcurrent relays are depicted in Fig. 13.

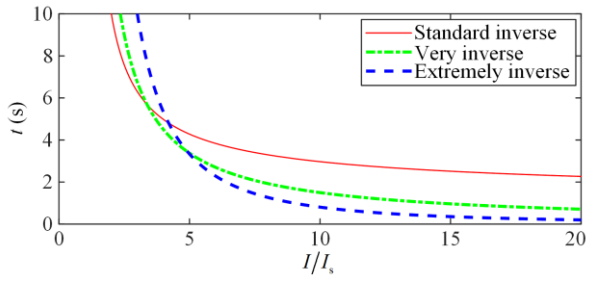

Fig. 13. The time-current characteristics of overcurrent relays.

The general expression can be written as [85]:

$$t = \frac{G}{\left(\left(I/I_s\right)^n - 1\right)} \tag{20}$$

where I denotes the actual fault current; I_s denotes the pickup current; and G and n are different for different inverse overcurrent relays, as shown in Table II [86].

TABLE II
PARAMETERS OF OVERCURRENT RELAYS

	G	n
Inverse time relays	0.14	0.02
Very inverse time relays	13.5	1
Extremely inverse time relays	80	2

IDMT overcurrent relays are the combination of defined time overcurrent relays and inverse time relays [87]. There is an inverse relationship between time and current for the smaller fault current, but the operating time is almost fixed for the higher fault current. When RESs are connected to the distribution network in Fig. 14, the main challenges for these overcurrent relays are as follows: 1) When a fault arises at F_1, the RES integration will increase the fault current flowing through the relay R_{12}, so that R_{12} may be erroneously activated. This means the protection coordination between R_{12} and R_{22} will have problems; 2) If the fault point is still at F_1, a fault current flows through R_{13} in the opposite direction, so R_{13} may have an unnecessary trip to enlarge the outrage; 3) For a fault at F_2, RESs will increase the voltage at Bus 3 during a fault, so the fault current flowing R_{13} will be reduced, and the sensitivity of overcurrent relays will be affected adversely [88]–[90]. In addition, the RES output power has high volatility since it is easily affected by weather conditions, making protection settings face challenges [91].

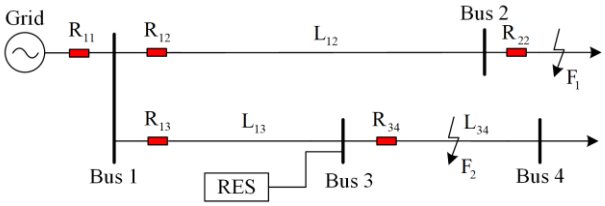

Fig. 14. A typical distribution network.

When the grid-connected breaker is open, RESs with the local load can form a microgrid if the output power from RESs matches the local load [92]. Since the fault current from CIRESs is limited, it is not enough to activate overcurrent relays [7]. For DFIGs, overcurrent relays also suffer from low fault current or non-fundamental components [26], [93].

In summary, traditional protection methods will suffer challenges after large-scale RESs are connected.

V. EXISTING SOLUTIONS

To solve protection problems, numerous new protec-

tion methods are proposed. They could be categorized into three parts: time-domain methods, frequency-domain methods, and active control-based methods.

A. Pilot Protection

For CIRESs, an equivalent differential impedance is defined by the ratio of the differential voltage to the differential current, and the magnitude feature could be utilized to distinguish internal faults from external faults [94]. The restrained impedance is mentioned in [95], and the differential impedance will be higher than the restraint impedance for internal faults, but its capability to withstand fault resistance is limited. Additionally, the fault current of CIRESs is far lower than that from the grid, so the current magnitude ratio between both sides is smaller than 1 for internal faults, but the ratio will be close to 1 for external faults [96], [97]. Furthermore, the positive- and negative-sequence current ratio is added to constitute a comprehensive criterion to improve the sensitivity, but the phase selection ability will disappear [98]. In addition, a new control strategy is designed to make the current angle difference less than 60°, so the sensitivity of differential protection can be improved [47]. For DFIGs with the crowbar activation, an effective method to extract the main frequency is used, and the current frequency disparity-based pilot protection is suggested in [99], but it is only applicable for the case with the crowbar input. Moreover, the frequency spectrum of the DFIG fault current is analyzed, and a differential protection method relying on the frequency spectrum index is proposed in [100].

Some methods can be applied to CIRESs and DFIGs. The fault current of RESs always has some differences in amplitude, frequency, phase angle, and harmonic amount, so some mathematical algorithms are used to evaluate the waveform similarity to constitute new pilot protection, such as Pearson correlation coefficient [101] and cosine similarity [35], [102]. Their performance is shown in Fig. 15 when a BC fault arises in the middle of the transmission line and the source type is CIRESs.

As shown in Fig. 15, the calculated value is higher than the threshold value quickly for the faulty phases, but lower than the setting value for the non-faulty phase, so these two methods can work properly. In addition, the sensitivity of the cosine similarity in Fig. 15(b) will be higher than the Pearson coefficient in Fig. 15(a) since there is no average term in the cosine similarity. They use the data window within 20 ms to avoid the power phasor extraction, but both are disabled when the fault current of CIRESs is equal to zero. To solve this issue, Spearman's rank correlation coefficient-based pilot protection is proposed in [34], but the rank processing method is different according to different fault current amplitudes, so an auxiliary criterion needs to be added to detect the fault current peak value. Another auxiliary criterion is added to compensate for this shortcoming for structural similarity-based pilot protection [103]. To use a unified criterion, a pilot protection scheme based on improved Euclidean distance has been put forward [30]. The parameter identification method is introduced into the protection field, and it relies on distinguishing whether the first-order derivative of the time-domain differential voltage and differential current align with the capacitance model [104], [105], However, the first derivative is susceptible to the influence of high harmonics, necessitating further enhancements to the performance of this method. In addition, some traveling wave-based pilot protection methods are proposed in [106]–[108], but they have a high sampling frequency requirement.

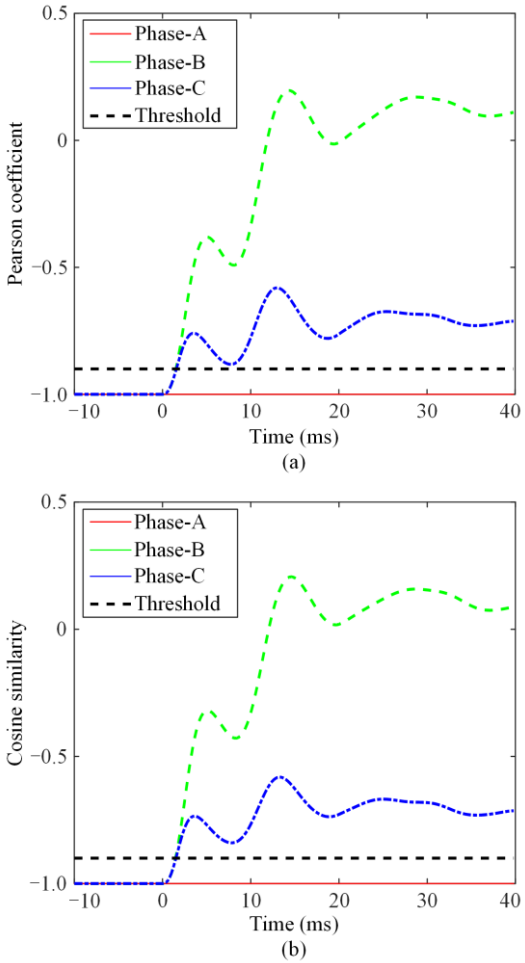

Fig. 15. The performance of Pearson coefficient and Cosine similarity. (a) Pearson coefficient. (b) Cosine similarity.

B. Directional Elements

Some effective methods are proposed for CIRESs to detect the fault direction. The equivalent sequence impedances of CIRESs are far higher than those of SGs, so the impedance feature is utilized to design a new directional relay [36]. Accordingly, the smaller fault current feature is used in [109]. Reference [65] points out that the latest standard VDE-AR-N 4120 can make the negative-sequence impedance of CIRESs behave like SGs, so negative-sequence directional elements can

work properly. When the filter capacitor is considered in the model establishment of the controller, a new control system is designed to adjust the negative-sequence equivalent impedance angle [44], but the above two methods cannot adjust the positive-sequence superimposed impedance. A new fault control strategy is formed in [73] to adjust the positive-sequence superimposed impedance angle of CIRESs equal to 90°, so positive-sequence fault component-based directional elements operate correctly. For DFIGs with crowbar activation, the fast decay feature of the DFIG fault current can be evaluated by calculating the difference between the first two peak-peak values, which is an effective method to distinguish the DFIG fault current from the grid fault current [26]. In this way, a direction detection method can be established.

In addition, some methods can be applied not only to CIRESs but also to DFIGs. The equivalent resistance is fitted by the least square method, and the sign of the evaluated resistance can be utilized to detect the fault direction [38], [110]. To overcome the dead zone problem for a fault occurring at the relay outlet, an auxiliary scheme is constructed by the correlation between the measured voltage dip and the calculated voltage dip [111]. However, the presence of a hard current limiter distorts the current waveform during the first quarter cycle, thereby impacting the performance of the protection scheme [112]. Another scheme is put forward in [113]–[115] based on the transient energy of the traveling wave, but a high sampling frequency is required. Moreover, high-frequency impedances of CIRESs and DFIGs are established in [23], [116], the impedance presents the inductive state in the high-frequency zone, but the used frequency should be explored further.

C. Phase Selectors

Phase selectors are also important protective relays. For CIRESs or DFIGs with no crowbar activation, the relative angle difference between sequence voltages satisfies the fixed relationship for different fault types, so this feature is used to construct a new phase selector [24]. Moreover, the current angle zone can be adjusted according to the calculated sequence impedance angles of the backside system, so an adaptive phase selector is proposed in [117]. In addition, the faulty phases can be determined by computing the correlation coefficient of phase transient voltage waveforms [118]. An initial traveling wave-based phase selector is proposed in [119], but it has a high sampling rate requirement. In addition, when the negative-sequence impedance angle is adjusted to 90°, the phase selector based on δ_0 can determine the fault type correctly, but δ_1 cannot come into the correct zone for the specific fault type [44]. In [43], the superimposed negative-sequence current angle is adjusted to respectively track the superimposed positive-sequence current angle and zero-sequence current angle, so δ_1 or δ_0 can operate correctly, but both cannot operate simultaneously. Moreover, the phase selector based on δ_1 and δ_0 can work properly if the positive and negative-sequence superimposed impedance angle is adjusted equal to 90° [73]. δ_1 is redefined as the sequence current relative angle difference instead of the superimposed sequence current angle difference, and a new controller is designed to make it operate correctly [40].

D. Distance Relays

Researchers pay more attention to the improvements in distance relays. Aimed at CIRESs, a new apparent impedance expression is constituted to reduce the influence of the weak infeed by amplifying the function of the zero-sequence current for asymmetrical ground faults, but this method is not applicable for non-grounding faults [109]. Reference [22] points out that the circuit breaker on the grid side can be allowed to trip first, so the remote infeed from the grid will disappear, but the grid-following inverter may not consistently produce a stable fault current at the fundamental frequency due to lack of voltage support from the grid. The operating characteristic is rotated clockwise or counterclockwise according to the voltage and current measured at different relay points to improve its performance, but distance relays will lose the original advantage of using only the local data [120], [121]. After establishing the circuit model of CIRESs, an adaptive distance relay is proposed in [122] only using the local information. However, this method adjusts the operating zone of distance relays according to the fault at the reach setting, so the protection range for zone-1 will be reduced, and zone-2 will be enlarged. In this way, zone-2 may lose coordination with zone-1 on the next line. Moreover, some methods based on active control are proposed for CIRESs. The fault current of CIRESs is controlled to 0 to eliminate the impact of the RES integration, but RESs should ride through the fault in modern grid codes [123]. The positive-sequence currents of SGs are mimicked by designing suitable current command values of the current control loop, so the apparent reactance is equal to the line fault reactance, and the quadrilateral protection zone with a large resistance reach can cover the large resistive component contained in the apparent impedance [42]. The positive-sequence circuit of CIRESs is equivalent to a voltage source with a constant impedance, and the negative-sequence fault circuit is modeled as an inductive impedance, so the current angle on both sides is similar such that the apparent reactance can reflect the fault distance [40]. However, the reactive current injection requirement is not achieved in the above two methods. This point is considered in [39], but some errors will be present between the apparent reactance and the actual line fault reactance. To combine the advantages of reactive current injection and apparent impedance calculation accuracy, Reference [124] proposes a novel control strategy. When

a BC fault with 20 Ω of R_g occurs in the middle of the line, the related measurements are illustrated in Fig. 16.

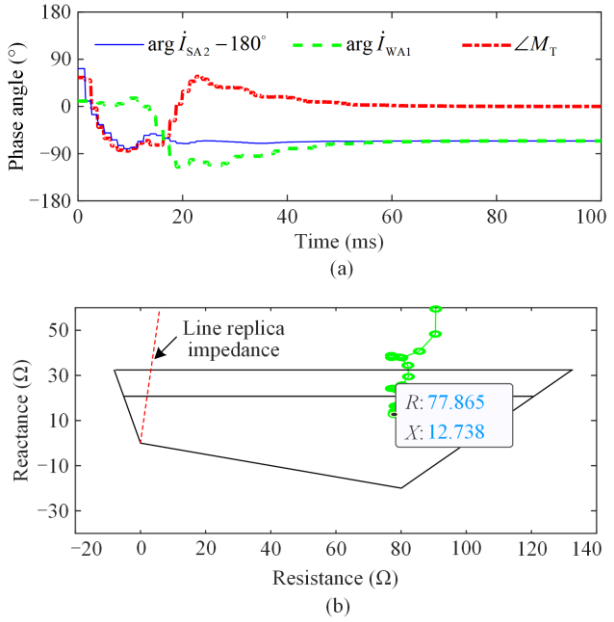

Fig. 16. The related measurements of distance relays. (a) Different angles. (b) Apparent impedance.

As displayed in Fig. 16(a), arg $\dot{I}_{WA1}$ can follow the (arg $\dot{I}_{SA2}$ −180°) when the developed FRT is executed. At this time, the apparent reactance in Fig. 16(b) will come into zone 1, and is also close to the line fault reactance. Additionally, the specific harmonic component can be generated by CIRESs, and distance relays can measure the harmonic impedance to reflect the fault distance since there is no harmonic component for the grid-side fault current during the steady state [41], [125], [126]. The harmonic injection can be achieved by the PI controller in [41], but the actual injection value will have some differences from the harmonic reference value. Moreover, accurate control can be realized by a proportional resonance (PR) controller in [41], [125], [126].

When the crowbar device of DFIGs is activated, the directional relay based on the fast decay of the DFIG fault current in [54] is used to prevent the local relay from tripping for the fault on the downstream line, so a modified permissive overreach transfer trip (POTT) scheme is constructed. In addition, some methods are general for CIRESs and DFIGs. The loop differential equation is established in [127], [128], and the least square method is used to evaluate the line inductance and calculate the fault distance using the data on both sides. In addition, traveling wave protection is effective in evaluating the fault distance, but accurate wavefront detection is the main challenge for these methods [129], [130]. In addition, they have high requirements for sampling cards. A high-frequency component-based distance protection method is developed in [37], [131], but the requirement for the sampling rate is also high for this method.

E. Overcurrent Relays

These methods to improve the function of overcurrent relays can be divided into non-communication relays and communication-assisted relays. For the first method, distribution generators (DGs) could be disconnected from the grid when the penetration of RESs is not high, so DGs do not undermine the performance of overcurrent relays [132]. However, modern grid codes require that DGs ride through a fault within a defined time. In addition, some scholars study a RES placement method to achieve maximum RES penetration under the premise that the relay operation is not affected [133]. The protection coordination is constructed as a linear programming (LP) problem, and a simplex algorithm is used to solve it [134]. This method provides one setting applicable for different DG output powers from zero to the rated capacity, but it may be difficult for some network topologies. Conversely, the protection coordination is modeled as a nonlinear programming (NLP) problem, and many techniques can be utilized to solve it such as the seeker optimization technique in [135] and the imperialistic competition algorithm in [136]. However, the DG uncertainty is not taken into account. Different orders of harmonics are injected into the distribution network from different DGs, and a new harmonic directional overcurrent relay is proposed in [137]. Distance relays are considered as a promising scheme for active distribution networks since it is less affected by the fault current level [138]. Moreover, the fault current limiter is used to restore the original fault current value after DGs are installed [139], [140].

The second method requires the installation of a central protection unit (CPU). The CPU can detect the changes in the system topology, the DG capacity, and the DG integration placement, and send new protection settings to relays in [141], [142], but it is infeasible to maintain numerous protection settings for all the system conditions. To solve this problem, all the possible system configurations are aggregated into a limited number of clusters, and a setting group is given for each cluster, so the critical problem is how to optimize the setting groups for this method. The k-means clustering-based method is used to cluster the network configurations, and a LP model is established to resolve the setting groups [143]. In addition, the differential searching algorithm is utilized to obtain the optimized setting group considering five possible distribution network structures [144]. Another two-step approach is proposed in [145], [146], The first step is to use the Genetic algorithm to cluster all the possible network configurations, and the second step is to linearize the protection coordination model. To obtain the optimal network cluster and the setting groups, the coordination issue is constructed as a

mixed-integer linear problem to compute the global optimum solution by CPU monitoring. Finally, the merits and demerits of different protective relays are summarized in Table III to compare these methods.

TABLE III
COMPARISONS AMONG DIFFERENT PROTECTION SCHEMES

Relay	Ref.	Type	Merits	Demerits
Pilot protection	[30], [34], [35], [95]–[99]	Time domain	1. Applicable for DFIGs and CIRESs. 2. Good ability to resist fault resistance.	1. Similarity-based pilot protection does not have a definite standard for the protection setting. 2. Differential term-based methods have a limited capacity to withstand noise.
	[100]–[102]	Traveling waves	1. Applicable for DFIGs and CIRESs. 2. Very fast operation speed. 3. Good ability to resist fault resistance.	1. Difficult to detect the initial traveling wave accurately. 2. High sampling rate requirement.
	[88]–[92]	Fundamental frequency	1. Easy to be used in protective devices. 2. Good ability to withstand noise interference.	1. Only applicable for CIRESs. 2. Some methods lose the ability for phase selection.
	[47]	Active control	1. Original traditional protective relays can operate with no or few revisions. 2. Applicable for different fault types, and power factors before a fault.	1. The reactive current injection is not satisfied for some methods. 2. Only applicable for CIRESs.
Directional elements	[38], [104], [105]	Time domain	1. Detect the fault direction for CIRESs and DFIGs. 2. Resist a high fault resistance.	1. Poor ability to resist noise. 2. Rely on the right mathematical model.
	[107]–[109]	Traveling waves	1. Fast speed for directional detection. 2. Applicable for different power converters.	1. Require a high sampling frequency. 2. Have difficulty in detecting the initial traveling wave. 3. Affected by the lightning wave
	[26], [36], [103]	Fundamental frequency	1. Easy to be updated in actual protective relays. 2. Resist a relatively large noise.	1. Some methods may be affected by the load current and rely on zero-sequence current for ground faults. 2. Only applicable for CIRESs.
	[23], [110]	High frequency	1. Applicable for DFIGs and CIRESs. 2. Good ability to resist fault resistance.	1. Rely on the detailed parameters of LCL. 2. High requirements for sampling frequencies.
	[44], [62], [69]	Active control	1. Make CIRESs compatible with directional elements. 2. Different fault types and points. 3. Current limiting of CIRESs can be satisfied.	1. Slow operation speed. 2. Controller may lose stability for severe faults. 3. Reactive current priority may be not satisfied for some methods.
Phase selector	[112]	Time-domain	1. Applied for DFIGs and CIRESs. 2. Good ability for fault resistance.	1. Difficult to set the threshold value. 2. High sampling rate.
	[113]	Traveling waves	1. Very fast operating speed. 2. Good ability for fault resistance.	1. High sampling rate. 2. Difficult to detect wave fronts.
	[24], [111]	Fundamental frequency	1. Easy to be used in actual protective relays. 2. Some methods are only applicable to CIRESs.	1. Some method is only applied for CIRESs.
	[40], [43], [44], [69]	Active control	1. Compatible with original phase selectors. 2. The current limiting for CIRESs can be satisfied.	1. Only for CIRESs. 2. Reactive current injection may not be satisfied.
Distance relays	[121], [122]	Time-domain	1. Not affected by the remote infeed. 2. Good ability to resist fault resistance.	1. Affected by noise interface. 2. High sampling rate. 3. High requirement for communication
	[123], [124]	Traveling waves	1. Fast operating speed. 2. Good ability for fault resistance.	1. High sampling frequency. 2. Affected by lighting waves.
	[22], [103], [114]–[116]	Fundamental frequency	1. A few revisions for traditional relays. 2. Less affected by the remote infeed.	1. Slow operating speed. 2. Some methods require remote data.
	[37], [125]	High frequency	1. Resist 30 dB of noise. 2. Not affected by frequency offset.	1. High sampling rate. 2. Suitable frequency range may be not found.
	[39]–[42], [54], [117], [119], [120]	Active control	1. For different fault types and fault points. 2. Make CIRESs compatible with traditional distance relays.	1. The apparent impedance still includes a big resistive component. 2. The control strategy may be not activated for high-resistance faults.
Overcurrent relays	[126]–[134]	Non-communication	1. Most methods are applicable for SG-based and inverter-based DGs. 2. Overcurrent relays can operate without any revision for some methods.	1. Some methods need extra devices. 2. Sometimes relay on the specific topology and RES location.
	[135]–[140]	Communication	1. Detect the system change in real time. 2. High reliability.	1. High requirement for communication. 2. Require a large investment for a distribution network.

VI. Future Perspectives

Through the review of fault characteristics and protection schemes, some future perspectives can be given.

A. The Accurate Fault Current Calculation for RESs

The fault current of CIRESs is determined by the DQ current references and the controller structure. The current references are given according to voltage sags. In the existing methods, the voltage transient is ignored, and the reference change during and before a fault is simplified as a step response, but the accurate current references should be close to a waveform that decays exponentially. The stator-side current of DFIGs is related to the current references of RSC when the crowbar device is not activated, so it also has the same problem. In addition, existing methods often aggregate the wind farm as a single wind turbine, but different wind turbines may detect different voltage dips for a fault such that they can have different FRT states. Therefore, the aggregation method should be optimized during the fault current calculation.

B. Advanced Mathematical Algorithm Application

The RES integration changes the fault signatures of the grid, so traditional fundamental frequency protection schemes may not work properly. Therefore, some mathematical morphological methods can extract new fault behaviors to construct new protection methods. In addition, some explainable machine learning or deep learning methods may also be used. The actual fault data is difficult to obtain, so the dataset is difficult to include all the fault conditions. Although the simulation can partly solve this problem, the simulation data is still different from the real power systems. Therefore, transferable intelligent algorithms may be a research hotspot.

C. Control Technology Application

In the future, the power grid can become a 100% renewable energy system. There will be so many converters that can be controlled, so it is easy to provide some special signals by designing the advanced controller, which is helpful for the correct operation of protective relays. However, these special signals from different power plants may interfere with each other, so how to achieve coordination control among different power plants will also be an interesting topic. In addition, the grid-forming controller will make CIRESs behave like SGs in many aspects, so new FRT strategies can be developed to ensure the safety of inverters and improve the protection function.

VII. Conclusions

The steady-state fault current of RESs can be easily calculated according to coordinate transformation. However, the transient current is uncontrollable and nonlinear. The PI controller and PLL will affect the transient current of CIRESs. In addition to the armature reaction, the RSC controller parameters and crowbar operation state will also lead to different transient behaviors for DFIGs.

The limited fault current of CIRESs will amplify the impact of the fault resistance so that distance relays will be affected. In addition, the controlled current angle may make the phase selector misjudge the fault type and differential protection has a declined sensitivity. For DFIGs, the current frequency offset will cause spectrum leakage, damaging the correct operation of phase selectors and differential protection. In addition, the terminal voltage is still at the power frequency, so the unstable measured impedance trajectory can lead to the misoperation of distance relays. Similarly, directional relays will also suffer due to the variable impedance feature of RESs. In addition, a brief problem overview is also given for overcurrent relays in the distribution networks

To solve these problems, numerous new protection methods are proposed. However, these approaches still have some drawbacks in terms of speed and sensitivity or have high sampling rate requirements. Since the power grid is being transformed to be a 100% renewable energy system, the control technologies and transient current-based protection schemes will play a more important role in maintaining system security in the future.

Acknowledgment

Zhe Yang thanks Dr. Zahid Javid at the Hong Kong Polytechnic University for his great help in polishing the language of this paper.

Authors' Contributions

Zhe Yang: full-text writing and the construction of the paper framework. Hongyi Wang: software and simulations. Wenlong Liao: methodology and visualization. Claus Leth Bak: supervision. Zhe Chen: supervision. All authors read and approved the final manuscript.

Funding

This work is carried out with the European Union's Horizon Research and Innovation Programme under Marie Skłodowska-Curie Grant Agreement (No. 101145934) and UKRI Postdoctoral Fellowships Guarantee (No. EP/Z002168/1).

Availability of Data and Materials

Please contact the corresponding author for data material requests.

Declarations

Competing interests: The authors declare that they

have no known competing financial interests or personal relationships that could have appeared to influence the work reported in this article.

AUTHORS' INFORMATION

Zhe Yang was born in China in 1994. He received a bachelor's degree in electrical engineering from Northeast Electric Power University in 2017, and a master's degree in electrical engineering from North China Electric Power University in 2020. After that, he obtained a Ph.D. degree in energy technology from AAU Energy at Aalborg University in 2023. He worked at the Hong Kong Polytechnic University from Sept. 2023 to Sept. 2024. He is currently a UKRI postdoctoral fellow at Imperial College London, and his research interests include power system protection and control, machine learning, and deep learning.

Hongyi Wang received the B.Eng. and M.S. degrees in electrical engineering from Shenyang University of Technology, Shenyang, China, in 2019. He is currently working toward the Ph.D. degree in power system with the Department of Energy Technology, Aalborg University, Aalborg, Denmark. His research interest is the modeling of wind farms.

Wenlong Liao received the B.S. degree in electrical engineering from China Agricultural University, Beijing, China, in 2017. He received the M.S. degree in electrical engineering from Tianjin University, Tianjin, China, in 2020 and the Ph.D. degree in energy technology from Aalborg University, Aalborg, Denmark, in 2023. Currently, he is a postdoc researcher with the Wind Engineering and Renewable Energy Laboratory, École Polytechnique Fédérale de Lausanne. His current research interests include smart grids, machine learning, and power system protection.

Claus Leth Bak was born in Arhus, Denmark, on April 13th, 1965. He received the B.Sc. with honors in electrical power engineering in 1992 and the M.Sc. in electrical power engineering at the Department of Energy Technology at Aalborg University in 1994. After his studies he worked as a professional engineer with electric power transmission and substations with specializations within the area of power system protection at the NV Net Transmission System Operator. In 1999 he was employed as an assistant professor at the Department of Energy Technology, Aalborg University. He received full professor position in 2011. He received the Ph.D. degree in 2015 with the thesis "EHV/HV underground cables in the transmission system." He has supervised/co-supervised +45 PhD's and +50 MSc theses. His main research areas include corona phenomena on overhead lines, composite transmission towers, power system modeling and transient simulations, underground cable transmission, power system harmonics, power system protection, composite materials for EHV power pylons and HVDC-VSC offshore transmission networks. He is the author/coauthor of app. 390 publications. He is chair of the Danish Cigré National Committee, member of CIGRE Technical Council and a member of Cigré SC C4 AG1. He received the DPSP 2014 Best Paper Award and the PEDG 2016 Best Paper Award. He received the CIGRE Distinguished member award (2020) and the CIGRE TC award (2020). He serves as head of the Energy Technology PhD program and as head of the Section of Electric Power Systems and Microgrids, and is a member of the PhD board at the Faculty of Engineering and Science.

Zhe Chen received the B.Eng. and M.Sc. degrees from the Northeast China Institute of Electric Power Engineering, Jilin, China, in 1982 and 1986, and the Ph.D. degree from the University of Durham, UK, in 1997. Dr. Chen is a full professor with the Department of Energy Technology, at Aalborg University, Denmark. He is the leader of Wind Power System Research program at the Department of Energy Technology, Aalborg University and the Danish Principle Investigator for Wind Energy of Sino-Danish Centre for Education and Research. His research areas are power systems, power electronics and electric machines, and his main current research interests are wind energy and modern power systems. He has led many research projects and has more than 500 publications in his technical fields.

REFERENCES

[1] W. Cui, Y. Jiang, and B. Zhang, "Reinforcement learning for optimal primary frequency control: a Lyapunov approach," *IEEE Transactions on Power Systems*, vol. 38, no. 2, pp. 1676-1688, Mar. 2023.

[2] S. Huang, L. Xiong, and Y. Zhou *et al*., (2024, May), "Distributed predefined-time control for power system with time delay and input saturation," *IEEE Transactions on Power Systems*, [Online], pp. 1-14. Available:https://ieeexplore.ieee.org/abstract/document/10533851

[3] Y. Yu, G. P. Liu, and Y. Huang *et al*., "Coordinated predictive secondary control for DC microgrids based on high-order fully actuated system approaches," *IEEE Transactions on Smart Grid*, vol. 15, no. 1, pp. 19-33, Jan. 2024.

[4] J. Jia, G. Yang, and A. H. Nielsen, "A review on grid-connected converter control for short-circuit power provision under grid unbalanced faults," *IEEE Transactions on Power Delivery*, vol. 33, no. 2, pp. 649-661, Apr. 2018.

[5] W. Xing, C. Hang, and W. Li *et al*., "Research on power supply ratio scheme of source network charging and

storage project under the dual carbon target," in *2021 IEEE International Conference on Electrical Engineering and Mechatronics Technology* (*ICEEMT*), Qingdao, China, 2021, pp. 294-300.

[6] Z. Chu and F. Teng, "Short circuit current constrained UC in high IBG-penetrated power systems," *IEEE Transactions on Power Systems*, vol. 36, no. 4, pp. 3776-3785, Jul. 2021.

[7] A. Hooshyar and R. Iravani, "Microgrid protection," *Proceedings of the IEEE,* vol. 105, no. 7, pp. 1332-1353, Jul. 2017.

[8] V. Telukunta, J. Pradhan, and A. Agrawal *et al*., "Protection challenges under bulk penetration of renewable energy resources in power systems: a review," *CSEE Journal of Power and Energy Systems,* vol. 3, no. 4, pp. 365-379, Dec. 2017.

[9] A. K. Pradhan and A. Routray, "Applying distance relay for voltage sag source detection," *IEEE Transactions on Power Delivery,* vol. 20, no. 1, pp. 529-531, Jan. 2005.

[10] S. Dambhare, S. A. Soman, and M. C. Chandorkar, "Adaptive current differential protection schemes for transmission-line protection," *IEEE Transactions on Power Delivery*, vol. 24, no. 4, pp. 1832-1841, Oct. 2009.

[11] IEEE Draft Guide for Protective Relay Applications to Transmission Lines, IEEE PC37.113/D8.0, 2015.

[12] S. Liu, L. Zhang, and C. Fu *et al*., "A new two-port network model-based pilot protection for AC transmission lines," *IEEE Transactions on Power Delivery*, vol. 35, no. 2, pp. 473-482, Apr. 2020.

[13] S. M. Hashemi and M. Sanaye-Pasand, "Current-based out-of-step detection method to enhance line differential protection," *IEEE Transactions on Power Delivery*, vol. 34, no. 2, pp. 448-456, Apr. 2019.

[14] S. Dechphung and T. Saengsuwan, "Three zones adaptive characteristic of the mho distance relay by KU method," in *2008 IEEE International Conference on Sustainable Energy Technologies*, Singapore, Singapore, 2008, pp. 1206-1210.

[15] S. H. Horowitz and A. G. Phadke, "Third zone revisited," *IEEE Transactions on Power Delivery*, vol. 21, no. 1, pp. 23-29, Jan. 2006.

[16] Z. Yang, K. Jia, and Z. Li *et al*., "Adaptability analysis of the directional relay for the system with inverter-interfaced renewable energy generators," in *2019 IEEE 8th International Conference on Advanced Power System Automation and Protection (APAP)*, Xi'an, China, 2019, pp. 1611-1616.

[17] J. Tang, G. Song, and C. Wang, "Adaptability analysis of directional relays in power systems with wind farms," in *13th International Conference on Development in Power System Protection 2016 (DPSP)*, Edinburgh, UK, 2016, pp. 1-6.

[18] J. C. Quispe and E. Orduña. "Transmission line protection challenges influenced by inverter-based resources: a review," *Protection and Control of Modern Power Systems,* vol. 7, no. 3, pp. 1-17, Jul. 2022.

[19] G. Benmouyal, M. Meisinger, and J. Burnwort *et al*., "IEEE standard inverse-time characteristic equations for overcurrent relays," *IEEE Transactions on Power Delivery*, vol. 14, no. 3, pp. 868-872, Jul. 1999.

[20] C. Wang, G. Song, and J. Tang, "Protection performance of traditional distance relays under wind power integration," in *13th International Conference on Development in Power System Protection 2016 (DPSP)*, Edinburgh, UK, 2016, pp. 1-5.

[21] M. N. I. Sarkar, L. G. Meegahapola, and M. Datta, "Reactive power management in renewable rich power grids: a review of grid-codes, renewable generators, support devices, control strategies and optimization algorithms," *IEEE Access*, vol. 6, pp. 41458-41489, 2018.

[22] Y. Fang, K. Jia, and Z. Yang *et al*., "Impact of inverter-interfaced renewable energy generators on distance protection and an improved scheme," *IEEE Transactions on Industrial Electronics*, vol. 66, no. 9, pp. 7078-7088, Sept. 2019.

[23] K. Jia, Z. Yang, and Y. Fang *et al*., "Influence of inverter-interfaced renewable energy generators on directional relay and an improved scheme," *IEEE Transactions on Power Electronics*, vol. 34, no. 12, pp. 11843-11855, Dec. 2019.

[24] A. Hooshyar, E. F. El-Saadany, and M. Sanaye-Pasand, "Fault type classification in microgrids including photovoltaic DGs," *IEEE Transactions on Smart Grid*, vol. 7, no. 5, pp. 2218-2229, Sept. 2016.

[25] A. Hooshyar, M. A. Azzouz, and E. F. El-Saadany, "Distance protection of lines emanating from full-scale converter-interfaced renewable energy power plants—part I: problem statement," *IEEE Transactions on Power Delivery*, vol. 30, no. 4, pp. 1770-1780, Aug. 2015.

[26] A. Hooshyar, M. A. Azzouz, and E. F. El-Saadany, "Three-phase fault direction identification for distribution systems with DFIG-based wind DG," *IEEE Transactions on Sustainable Energy*, vol. 5, no. 3, pp. 747-756, Jul. 2014.

[27] B. Mahamedi, M. Eskandari, and J. E. Fletcher *et al*., "Sequence-based control strategy with current limiting for the fault ride-through of inverter-interfaced distributed generators," *IEEE Transactions on Sustainable Energy*, vol. 11, no. 1, pp. 165-174, Jan. 2020.

[28] J. Ma, D. Zhao, and L. Yao *et al*, "Analysis on application of a current-source based DFIG wind generator model," *CSEE Journal of Power and Energy Systems*, vol. 4, no. 3, pp. 352-361, Sept. 2018.

[29] Z. Zhang, Y. Zhao, and W. Qia *et al*., "A discrete-time direct torque control for direct-drive PMSG-based wind energy conversion systems," in *IEEE Transactions on Industry Applications*, vol. 51, no. 4, pp. 3504-3514, Aug. 2015.

[30] Z. Yang, W. Liao, and H. Wang *et al*., "Improved euclidean distance based pilot protection for lines with renewable energy sources," *IEEE Transactions on Industrial Informatics*, vol. 18, no. 12, pp. 8551-8562, Dec. 2022.

[31] D. Shin, K. J. Lee, and J. P. Lee *et al*., "Implementation

of fault ride-through techniques of grid-connected inverter for distributed energy resources with adaptive low-pass notch PLL," *IEEE Transactions on Power Electronics*, vol. 30, no. 5, pp. 2859-2871, May 2015.

[32] Z. Zou, X. Xiao, and Y. Liu *et al*., "Integrated protection of DFIG-based wind turbine with a resistive-type SFCL under symmetrical and asymmetrical faults," *IEEE Transactions on Applied Superconductivity*, vol. 26, no. 7, pp. 1-5, Oct. 2016.

[33] S. Gao, K. Yu, and G. Song, "Calculation and protection method for a three-phase short circuit fault current based on a doubly-fed wind field," *Power System Protection and Control*, vol. 51, no. 7, pp. 32-39, Apr. 2023. (in Chinese)

[34] K. Jia, Z. Yang, and L. Zheng *et al*., "Spearman correlation-based pilot protection for transmission line connected to PMSGs and DFIGS," *IEEE Transactions on Industrial Informatics*, vol. 17, no. 7, pp. 4532-4544, Jul. 2021.

[35] L. Zheng, K. Jia, and T. Bi *et al*., "Cosine similarity based line protection for large-scale wind farms," *IEEE Transactions on Industrial Electronics*, vol. 68, no. 7, pp. 5990-5999, Jul. 2021.

[36] A. Hooshyar and R. Iravani, "A new directional element for microgrid protection," *IEEE Transactions on Smart Grid*, vol. 9, no. 6, pp. 6862-6876, Nov. 2018.

[37] Z. Yang, K. Jia, and Y. Fang *et al*., "High-frequency fault component-based distance protection for large renewable power plants," *IEEE Transactions on Power Electronics*, vol. 35, no. 10, pp. 10352-10362, Oct. 2020.

[38] C. Wang, G. Song, and J. Zhang, "A novel principle of directional relay for wind power integration based on model recognition in time-domain," in *2016 IEEE PES Asia-Pacific Power and Energy Engineering Conference (APPEEC)*, Xi'an, China, 2016, pp. 1851-1855.

[39] K. Ma, Z. Chen, and Z. Liu *et al*., "Protection collaborative fault control for power electronic-based power plants during unbalanced grid faults," *International Journal of Electrical Power & Energy Systems*, vol. 130, Sept. 2021.

[40] A. Banaiemoqadam, A. Hooshyar, and M. A. Azzouz, "A comprehensive dual current control scheme for inverter-based resources to enable correct operation of protective relays," *IEEE Transactions on Power Delivery*, vol. 36, no. 5, pp. 2715-2729, Oct. 2021.

[41] Z. Yang, Q. Zhang, and W. Liao *et al*., "Harmonic injection based distance protection for line with converter-interfaced sources," *IEEE Transactions on Industrial Electronics*, vol. 70, no. 2, pp. 1553-1564, Feb. 2023.

[42] A. Banaiemoqadam, A. Hooshyar, and M. A. Azzouz, "A control-based solution for distance protection of lines connected to converter-interfaced sources during asymmetrical faults," *IEEE Transactions on Power Delivery*, vol. 35, no. 3, pp. 1455-1466, Jun. 2020.

[43] M. A. Azzouz and A. Hooshyar, "Dual current control of inverter-interfaced renewable energy sources for precise phase selection," *IEEE Transactions on Smart Grid*, vol. 10, no. 5, pp. 5092-5102, Sept. 2019.

[44] M. A. Azzouz, A. Hooshyar, and E. F. El-Saadany, "Resilience enhancement of microgrids with inverter-interfaced DGs by enabling faulty phase selection," *IEEE Transactions on Smart Grid*, vol. 9, no. 6, pp. 6578-6589, Nov. 2018.

[45] Q. Zhang, D. Liu, and Z. Liu, *et al*., "Fault modeling and analysis of grid-connected inverters with decoupled sequence control," *IEEE Transactions on Industrial Electronics*, vol. 69, no. 6, pp. 5782-5792, Jun. 2022.

[46] Y. Wu, H. Wu, and F. Zhao *et al*., "Influence of PLL on stability of interconnected grid-forming and grid-following converters," *IEEE Transactions on Power Electronics*, vol. 39, no. 10, pp. 11980-11985, Oct. 2024.

[47] Z. Yang, W. Liao, and C. L. Bak, *et al*., "Fault coordination control for converter-interfaced sources compatible with differential protection during asymmetrical faults," *Energy Reports*, vol. 8, pp. 249-258, Nov. 2022.

[48] Z. Yang, R. Zhu, and W. Liao, "Minkowski distance based pilot protection for tie lines between offshore wind farms and MMC," *IEEE Transactions on Industrial Informatics*, vol. 20, no. 6, pp. 8441-8452, Jun. 2024.

[49] Q. Liu, K. Jia, and B. Yang *et al*., "Fault analysis of inverter-interfaced RESs considering decoupled sequence control," *IEEE Transactions on Industrial Electronics*, vol. 70, no. 5, pp. 4820-4830, May 2023.

[50] J. Svensson, M. Bongiorno, and A. Sannino, "Practical implementation of delayed signal cancellation method for phase-sequence separation," *IEEE Transactions on Power Delivery*, vol. 22, no. 1, pp. 18-26, Jan. 2007.

[51] H.-S. Song and K. Nam, "Dual current control scheme for PWM converter under unbalanced input voltage conditions," *IEEE Transactions on Industrial Electronics*, vol. 46, no. 5, pp. 953-959, Oct. 1999.

[52] A. Haddadi, M. Zhao, and I. Kocar *et al*., "Impact of inverter-based resources on negative sequence quantities-based protection elements," *IEEE Transactions on Power Delivery*, vol. 36, no. 1, pp. 289-298, Feb. 2021.

[53] W. Tang, J. Hu, and Y. Chang *et al*., "Modeling of DFIG-Based wind turbine for power system transient response analysis in rotor speed control timescale," in *ieee transactions on power systems*, vol. 33, no. 6, pp. 6795-6805, Nov. 2018.

[54] A. Hooshyar, M. A. Azzouz, and E. F. El-Saadany, "Distance protection of lines connected to induction generator-based wind farms during balanced faults," *IEEE Transactions on Sustainable Energy*, vol. 5, no. 4, pp. 1193-1203, Oct. 2014.

[55] G. Pannell, B. Zahawi, and D. J. Atkinson *et al*, "Evaluation of the performance of a dc-link brake chopper as a DFIG low-voltage fault-ride-through device," *IEEE Transactions on Energy Conversion*, vol. 28, no. 3, pp. 535-542, Sept. 2013.

[56] P.-H. Huang, M. S. El Moursi, and S. A. Hasen, "Novel fault ride-through scheme and control strategy for doubly fed induction generator-based wind turbine," *IEEE Transactions on Energy Conversion*, vol. 30, no. 2, pp.

635-645, Jun. 2015.

[57] X. Kong, Z. Zhang, and X. Yin *et al*., "Study of fault current characteristics of the DFIG considering dynamic response of the RSC," *IEEE Transactions on Energy Conversion*, vol. 29, no. 2, pp. 278-287, Jun. 2014.

[58] Y. Chang, I. Kocar, and E. Farantatos *et al.*, "Short-circuit modeling of DFIG-based WTG in sequence domain considering various fault ride-through requirements and solutions," *IEEE Transactions on Power Delivery*, vol. 38, no. 3, pp. 2088-2100, Jun. 2023.

[59] IEEE Standard for Interconnection and Interoperability of Inverter-Based Resources (IBRs) Interconnecting with Associated Transmission Electric Power Systems, IEEE Std 2800-2022, 2022.

[60] P. Piya, M. Ebrahimi, and M. Karimi-Ghartemani *et al*., "Fault ride-through capability of voltage-controlled inverters," *IEEE Transactions on Industrial Electronics*, vol. 65, no. 10, pp. 7933-7943, Oct. 2018.

[61] P. Wang, J. Song, and F. Lian *et al*., "Equivalent model of multi-type distributed generators under faults with fast-iterative calculation method based on improved PSO algorithm," *Protection and Control of Modern Power Systems*, vol. 6, no. 3, pp. 1-12, Jul. 2021.

[62] Z. Yang, Q. Zhang, and Z. Liu *et al*., "Fault current calculation for inverter-interfaced power sources considering saturation element," in *2021 IEEE 4th International Electrical and Energy Conference (CIEEC)*, Wuhan, China, 2021, pp. 1-5.

[63] K. Jia, Q. Liu, and B. Yang *et al*., "Transient fault current analysis of IIRESs considering controller saturation," *IEEE Transactions on Smart Grid*, vol. 13, no. 1, pp. 496-504, Jan. 2022.

[64] K. Jia, L. Hou, and Q. Li *et al*., "Analytical calculation of transient current from an inverter-interfaced renewable energy," *IEEE Transactions on Power Systems*, vol. 37, no. 2, pp. 1554-1563, Mar. 2022.

[65] A. Haddadi, I. Kocar, and J. Mahseredjian *et al*., "Negative sequence quantities-based protection under inverter-based resources challenges and impact of the German grid code," *Electric Power Systems Research*, vol. 188, Nov. 2020.

[66] P. Sochor, N. M. L. Tan, and H. Akagi, "low-voltage-ride-through control of a modular multilevel single-delta bridge-cell (SDBC) inverter for utility-scale photovoltaic systems," *IEEE Transactions on Industry Applications*, vol. 54, no. 5, pp. 4739-4751, Oct. 2018.

[67] M. A. G. López, J. L. G. de Vicuña, and J. Miret *et al*., "Control strategy for grid-connected three-phase inverters during voltage sags to meet grid codes and to maximize power delivery capability," *IEEE Transactions on Power Electronics*, vol. 33, no. 11, pp. 9360-9374, Nov. 2018.

[68] A. Azizi, A. Banaiemoqadam, and A. Hooshyar *et al*., "A blind spot in the lvrt current requirements of modern grid codes for inverter-based resources," *IEEE Transactions on Power Delivery*, vol. 38, no. 1, pp. 319-334, Feb. 2023.

[69] A. Varga, "Balancing free square-root algorithm for computing singular perturbation approximations," in *[1991] Proceedings of the 30th IEEE Conference on Decision and Control*, Brighton, UK, 1991, pp. 1062-1065.

[70] N. D. Tleis, "5-modelling of ac rotating machines," in *Newnes Power Engineering Series*, Oxford, UK: Newnes, 2008, pp. 301-396.

[71] Y. Liang, Y. Ren, and J. Yu *et al*., "Current trajectory image-based protection algorithm for transmission lines connected to MMC-HVDC stations using CA-CNN," *Protection and Control of Modern Power Systems*, vol. 8, no. 1, pp. 1-15, Jan. 2023.

[72] Y. Chang, M. Zhao, and I. Kocar, "The impact of DFIG control schemes on the negative-sequence based differential protection," *Electric Power Systems Research*, vol. 211, Oct. 2022.

[73] Z. Yang, Z. Liu, and Q. Zhang *et al*., "A control method for converter-interfaced sources to improve operation of directional protection elements," *IEEE Transactions on Power Delivery*, vol. 38, no. 1, pp. 642-654, Feb. 2023.

[74] R. Chowdhury and N. Fischer, "Transmission line protection for systems with inverter-based resources- part I: problems," *IEEE Transactions on Power Delivery*, vol. 36, no. 4, pp. 2416-2425, Aug. 2021.

[75] H. Nian, B. Hu, and Y. Xu *et al*., "Analysis and reshaping on impedance characteristic of DFIG system based on symmetrical PLL," *IEEE Transactions on Power Electronics*, vol. 35, no. 11, pp. 11720-11730, Nov. 2020.

[76] B. Hu, H. Nian, and M. Li *et al*., "Impedance characteristic analysis and reshaping method of DFIG system based on DPC without PLL," *IEEE Transactions on Industrial Electronics*, vol. 68, no. 10, pp. 9767-9777, Oct. 2021.

[77] X. Li, Y. Lu, and T. Huang, "Impact of the DFIG-based wind farm connection on the fault component-based directional relay and a mitigation countermeasure," *Energies*, vol. 13, no. 17. Aug. 2020.

[78] T. Adu, "An accurate fault classification technique for power system monitoring devices," *IEEE Transactions on Power Delivery*, vol. 17, no. 3, pp. 684-690, Jul. 2002.

[79] L. Zou, Q. Zhao, and X. Lin *et al*., "Improved phase selector for unbalanced faults during power swings using morphological technique," *IEEE Transactions on Power Delivery*, vol. 21, no. 4, pp. 1847-1855, Oct. 2006.

[80] S. Shen and P. Zhang, "Characteristics of sequence impedances of DFIG wind farm and the impacts on the phase selection elements," in *2014 IEEE PES General Meeting | Conference & Exposition,* National Harbor, MD, USA, 2014, pp. 1-5.

[81] W. O. Kennedy, B. J. Gruell, and C. H. Shih *et al*., "Five years experience with a new method of field testing cross and quadrature polarized mho distance relays. I. results and observations," *IEEE Transactions on Power Delivery*, vol. 3, no. 3, pp. 880-886, Jul. 1988.

[82] A. Banaiemoqadam, A. Azizi, and A. Hooshyar *et al*., "Impact of inverter-based resources on different implementation methods for distance relays—Part I: phase comparators," *IEEE Transactions on Power Delivery*, vol. 38, no. 6, pp. 4090-4102, Dec. 2023.

[83] A. Banaiemoqadam, A. Azizi, and A. Hooshyar *et al*., "Impact of inverter-based resources on different implementation methods for distance relays—part II: reactance method," *IEEE Transactions on Power Delivery*, vol. 38, no. 6, pp. 4049-4060, Dec. 2023.

[84] R. M. Chabanloo, H. A. Abyaneh, and S. S. H. Kamangar *et al*., "Optimal combined overcurrent and distance relays coordination incorporating intelligent overcurrent relays characteristic selection," *IEEE Transactions on Power Delivery*, vol. 26, no. 3, pp. 1381-1391, Jul. 2011.

[85] J. Chung, Y. Lu, and W. Kao *et al*., "Study of solving the coordination curve intersection of inverse-time overcurrent relays in subtransmission systems," *IEEE Transactions on Power Delivery*, vol. 23, no. 4, pp. 1780-1788, Oct. 2008.

[86] H. C. Kiliçkiran, İ. Şengör, and H. Akdemir *et al*., "Power system protection with digital overcurrent relays: a review of non-standard characteristics," *Electric Power Systems Research*, vol. 164, pp. 89-102, Nov. 2018.

[87] S. Acharya, S. K. Jha, and R. Shrestha *et al*., "An analysis of time current characteristics of adaptive inverse definite minimum time (IDMT) overcurrent relay for symmetrical and un-symmetrical faults," in *2017 International Conference on Smart grids, Power and Advanced Control Engineering (ICSPACE)*, Bangalore, India, 2017, pp. 332-337.

[88] J. S. Farkhani, M. Zareein, and H. Soroushmehr *et al*., "Coordination of directional overcurrent protection relay for distribution network with embedded DG," in *2019 5th Conference on Knowledge Based Engineering and Innovation (KBEI)*, Tehran, Iran, 2019, pp. 281-286.

[89] F. Motabarian, M. A. Golkar, and S. Hajiaghasi, "Surveying the effect of distributed generation (DG) on over current protection in radial distribution systems," in *18th Electric Power Distribution Conference,* Kermanshah, Iran, 2013, pp. 1-6.

[90] S. W. H. de Haan, "Impact of distributed generation units with power electronic converters on distribution network protection," in *2008 IET 9th International Conference on Developments in Power System Protection (DPSP 2008),* Glasgow, UK, 2008, pp. 664-669.

[91] P. Sookrod and P. Wirasanti, "Overcurrent relay coordination tool for radial distribution systems with distributed generation," in *2018 5th International Conference on Electrical and Electronic Engineering (ICEEE),* Istanbul, Turkey, 2018, pp. 13-17.

[92] R. H. Lasseter, "Smart distribution: coupled microgrids," in *Proceedings of the IEEE*, vol. 99, no. 6, pp. 1074-1082, Jun. 2011.

[93] J. Martínez, P. C. Kjær, and P. Rodriguez *et al*., "Short circuit signatures from different wind turbine generator types," in *2011 IEEE/PES Power Systems Conference and Exposition*, Phoenix, USA, 2011, pp. 1-7.

[94] T. G. Bolandi, H. Seyedi, and S. M. Hashemi *et al*., "Impedance-differential protection: a new approach to transmission-line pilot protection," *IEEE Transactions on Power Delivery*, vol. 30, no. 6, pp. 2510-2518, Dec. 2015.

[95] G. Chen, Y. Liu, and Q. Yang, "An impedance-based protection principle for active distribution network," in *2018 China International Conference on Electricity Distribution (CICED)*, Tianjin, China, 2018, pp. 1241-1245.

[96] K. Jia, Z. Yang, and Y. Fang *et al*., "Amplitude comparison based pilot protection for renewable power teed line," *CSEE Journal of Power and Energy Systems*, vol. 8, no. 6, pp. 1519-1529, Nov. 2022.

[97] K. Jia, Z. Yang, and Z. Zhu *et al*., "Current amplitude ratio based pilot protection for the transmission line connected to inverter-interfaced renewable energy power plants," in *2019 IEEE Innovative Smart Grid Technologies-Asia (ISGT Asia),* Chengdu, China, 2019, pp. 2090-2094.

[98] Z. Yang, W. Liao, and C. L. Bak *et al*., "Comprehensive current amplitude ratio based pilot protection for line with converter-interfaced sources," *Energy Reports*, vol. 8, pp. 420-430, Nov. 2022.

[99] N. Cao, T. Ge, and Q. Yu, "Research on main transformer protection of doubly-fed wind farm based on fault current frequency difference," in *2018 Chinese Automation Congress (CAC)*, Xi'an, China, 2018, pp. 4067-4072.

[100] X. Li and Y. Lu, "Improved amplitude differential protection scheme based on the frequency spectrum index for distribution networks with dfig-based wind DGs," *IEEE Access*, vol. 8, pp. 64225-64237, 2020.

[101] K. Jia, Y. Li, and Y. Fang *et al*., "Transient current similarity based protection for wind farm transmission lines," *Applied Energy*, vol. 225, pp. 42-51, Sept. 2018.

[102] L. Zheng, K. Jia, and W. Wu *et al*. "Cosine similarity based line protection for large scale wind farms part II—the industrial application," *IEEE Transactions on Industrial Electronics*, vol. 69, no. 3, pp. 2599-2609, Mar. 2022.

[103] L. Zheng, K. Jia, and T. Bi *et al*., "A novel structural similarity based pilot protection for renewable power transmission line," *IEEE Transactions on Power Delivery*, vol. 35, no. 6, pp. 2672-2681, Dec. 2020.

[104] X. Kang, J. Suonan, and G. Song *et al*., "Protection technique based on parameter identification-its principle and application," in *2008 IEEE Power and Energy Society General Meeting-Conversion and Delivery of Electrical Energy in the 21st Century*, Pittsburgh, USA, 2008, pp. 1-6.

[105] X. Kang, Z. Wu, and J. Suonan *et al*., "Research on pilot differential protection based on parameter identification and suitable frequency band of transmission line model," in *2011 International Conference on Advanced Power System Automation and Protection*, Beijing, China, 2011, pp. 234-241.

[106] Z. Ying, T. Nengling, and X. Bin, "Travelling wave-based

pilot direction comparison protection for HVDC line," *International Transactions on Electrical Energy Systems*, vol. 23, no. 8, pp. 1304-1316, Nov. 2013.

[107] D. Wang, M. Hou, and M. Gao *et al*., "Travelling wave directional pilot protection for hybrid HVDC transmission line," *International Journal of Electrical Power & Energy Systems*, vol. 107, pp. 615-627, May 2019.

[108] L. Jiang, Q. Chen, and W. Huang *et al*., "A novel directional pilot protection method for VSC-MTDC based on the initial forward and backward travelling wave head," *International Journal of Electrical Power & Energy Systems*, vol. 109, pp. 198-206, Jul. 2019.

[109] A. Hooshyar, M. A. Azzouz, and E. F. El-Saadany, "Distance protection of lines emanating from full-scale converter-interfaced renewable energy power plants—part II: solution description and evaluation," *IEEE Transactions on Power Delivery*, vol. 30, no. 4, pp. 1781-1791, Aug. 2015.

[110] G. Suryanarayana, G. Kesava Rao, and S. Sarangi *et al*., "Directional relaying using parameter estimation approach," *International Journal of Electrical Power & Energy Systems*, vol. 107, pp. 597-604, May 2019.

[111] X. Wang, M. Wen, and J. Zheng *et al.*, "A novel directional relay for AC lines close to the HVDC installation," *International Journal of Electrical Power & Energy Systems*, vol. 118, Jun. 2020.

[112] H. Jafarabadi Ashtiani, H. Samet, and T. Ghanbari, "Evaluation of directional relay algorithms in the presence of FCL," *IET Science*, *Measurement & Technology*, vol. 11, no. 6, pp. 713-722, Sept. 2017.

[113] L. Hao, D. Jiandong, and L. Yang *et al*., "Ultra-high-speed transient-based directional relay for AC transmission lines connected to LCC-HVDC inverter station," *International Journal of Electrical Power & Energy Systems*, vol. 123, Dec. 2020.

[114] C. Aguilera, E. Orduna, and G. Ratta, "Directional traveling-wave protection based on slope change analysis," *IEEE Transactions on Power Delivery*, vol. 22, no. 4, pp. 2025-2033, Oct. 2007.

[115] Z. He, X. Liu, and X. Li *et al*., "A novel traveling-wave directional relay based on apparent surge impedance," *IEEE Transactions on Power Delivery*, vol. 30, no. 3, pp. 1153-1161, Jun. 2015.

[116] K. Jia, T. Bi, and Z. Ren *et al*., "High frequency impedance based fault location in distribution system with DGs," *IEEE Transactions on Smart Grid*, vol. 9, no. 2, pp. 807-816, Mar. 2018.

[117] A. A. Aboelnaga and M. A. Azzouz, "Adaptive current-angle-based phase selection for microgrids with inverter-interfaced renewable energy sources," *IEEE Transactions on Smart Grid*, vol. 13, no. 1, pp. 417-428, Jan. 2022.

[118] G. Song, C. Wang, and T. Wang *et al*, "A phase selection method for wind power integration system using phase voltage waveform correlation," *IEEE Transactions on Power Delivery*, vol. 32, no. 2, pp. 740-748, Apr. 2017.

[119] X. Dong, W. Kong, and T. Cui, "Fault classification and faulted-phase selection based on the initial current traveling wave," *IEEE Transactions on Power Delivery*, vol. 24, no. 2, pp. 552-559, Apr. 2009.

[120] Y. Q. Xia, K. K. Li, and A. K. David, "Adaptive relay setting for stand-alone digital distance protection," *IEEE Transactions on Power Delivery*, vol. 9, no. 1, pp. 480-491, Jan. 1994.

[121] D. Pal, B. Mallikarjuna, and R. J. Reddy *et al.*, "Synchrophasor assisted adaptive relaying methodology to prevent zone-3 mal-operation during load encroachment," *IEEE Sensors Journal*, vol. 17, no. 23, pp. 7713-7722, Dec. 2017.

[122] K. Ma, H. K. Høidalen, and Z. Chen *et al*., "Improved zone 1 top-line tilting scheme for the polygonal distance protection in the outgoing line," *CSEE Journal of Power and Energy Systems*, vol. 9, no. 1, pp. 172-184, Jan. 2023.

[123] Z. Liu, H. K. Hoidalen, and M. M. Saha, "An intelligent coordinated protection and control strategy for distribution network with wind generation integration," *CSEE Journal of Power and Energy Systems*, vol. 2, no. 4, pp. 23-30, Dec. 2016.

[124] Z. Yang, W. Liao, and Q. Zhang *et al*., "Fault coordination control for converter-interfaced sources compatible with distance protection during asymmetrical faults," *IEEE Transactions on Industrial Electronics*, vol. 70, no. 7, pp. 6941-6952, Jul. 2023.

[125] K. A. Saleh and M. A. Allam, "Synthetic harmonic distance relaying for inverter-based islanded microgrids," *IEEE Open Access Journal of Power and Energy*, vol. 8, pp. 258-267, 2021.

[126] K. Jia, J. Chen, and Z. Xuan *et al*., "Active protection for photovoltaic DC-boosting integration system during FRT," *IET Generation*, *Transmission & Distribution*, vol. 13, no. 18, pp. 4081-4088, Sept. 2019.

[127] P. Adhikari, S. M. Brahma, and P. H. Gadde, "Source-agnostic time-domain distance relay," *IEEE Transactions on Power Delivery*, vol. 37, no. 5, pp. 3620-3629, Oct. 2022.

[128] S. J. Zubić, M. B. Djurić, and Č. V Zeljković, "Probabilistic assessment of new time-domain distance relay algorithms," *Electric Power Systems Research*, vol. 119, pp. 218-227, Feb. 2015.

[129] P. A. Crossley and P. G. McLaren, "Distance protection based on traveling waves," *IEEE Power Engineering Review*, vol. 3, no. 9, pp. 30-31, Sept. 1983.

[130] R. L. d. S. França, F. C. d. S. Júnior, and T. R. Honorato *et al*., "Traveling wave-based transmission line earth fault distance protection," *IEEE Transactions on Power Delivery*, vol. 36, no. 2, pp. 544-553, Apr. 2021.

[131] K. Jia, Q. Zhao, and T. Feng *et al*., "Distance protection scheme for dc distribution systems based on the high-frequency characteristics of faults," *IEEE Transactions on Power Delivery*, vol. 35, no. 1, pp. 234-243, Feb. 2020.

[132] IEEE Standard for Interconnecting Distributed Resources with Electric Power Systems, IEEE Std 1547-2003, 2003.

[133] H. Zhan, C. Wang, and Y. Wang *et al*., "Relay protection

coordination integrated optimal placement and sizing of distributed generation sources in distribution networks," *IEEE Transactions on Smart Grid*, vol. 7, no. 1, pp. 55-65, Jan. 2016.

[134]Ł. Huchel and H. H. Zeineldin, "Planning the coordination of directional overcurrent relays for distribution systems considering DG," *IEEE Transactions on Smart Grid*, vol. 7, no. 3, pp. 1642-1649, May 2016.

[135]T. Amraee, "Coordination of directional overcurrent relays using seeker algorithm," *IEEE Transactions on Power Delivery*, vol. 27, no. 3, pp. 1415-1422, Jul. 2012.

[136]P. Alaee and T. Amraee, "Optimal coordination of directional overcurrent relays in meshed active distribution network using imperialistic competition algorithm," *Journal of Modern Power Systems and Clean Energy*, vol. 9, no. 2, pp. 416-422, Mar. 2021.

[137]K. A. Saleh and A. Mehrizi-Sani, "Harmonic directional overcurrent relay for islanded microgrids with inverter-based DGs," *IEEE Systems Journal*, vol. 15, no. 2, pp. 2720-2731, Jun. 2021.

[138]A. Adrianti, A. R. Sijabat, and M. Nasir, "Analyzing performance of distance relay in protecting distribution lines with distributed generation," *2019 International Conference on Electrical Engineering and Computer Science (ICECOS)*, Batam, Indonesia, 2019, pp. 283-286.

[139]H. Yamaguchi and T. Kataoka, "Current limiting characteristics of transformer type superconducting fault current limiter with shunt impedance and inductive load," *IEEE Transactions on Applied Superconductivity*, vol. 18, no. 2, pp. 668-671, Jun. 2008.

[140]Y. Zhang and R. A. Dougal, "Novel dual-FCL connection for adding distributed generation to a power distribution utility," *IEEE Transactions on Applied Superconductivity*, vol. 21, no. 3, pp. 2179-2183, Jun. 2011.

[141]R. Jain, D. L. Lubkeman, and S. M. Lukic, "Dynamic adaptive protection for distribution systems in grid-connected and islanded modes," *IEEE Transactions on Power Delivery*, vol. 34, no. 1, pp. 281-289, Feb. 2019.

[142]M. Y. Shih, C. A. Castillo Salazar, and A. Conde Enríquez, "Adaptive directional overcurrent relay coordination using ant colony optimisation," *IET Generation, Transmission & Distribution*, vol. 9, no. 14, pp. 2040-2049, Nov. 2015.

[143]M. Ojaghi and V. Mohammadi, "Use of clustering to reduce the number of different setting groups for adaptive coordination of overcurrent relays," *IEEE Transactions on Power Delivery*, vol. 33, no. 3, pp. 1204-1212, Jun. 2018.

[144]M. Singh, T. Vishnuvardhan, and S. G. Srivani, "Adaptive protection coordination scheme for power networks under penetration of distributed energy resources," *IET Generation, Transmission & Distribution*, vol. 10, no. 15, pp. 3919-3929, Nov. 2016.

[145]E. Purwar, D. N. Vishwakarma, and S. P. Singh, "A novel constraints reduction-based optimal relay coordination method considering variable operational status of distribution system with DGs," *IEEE Transactions on Smart Grid*, vol. 10, no. 1, pp. 889-898, Jan. 2019.

[146]M. Ghotbi-Maleki, R. M. Chabanloo, and H. H. Zeineldin *et al*., "Design of setting group-based overcurrent protection scheme for active distribution networks using MILP," *IEEE Transactions on Smart Grid*, vol. 12, no. 2, pp. 1185-1193, Mar. 2021.